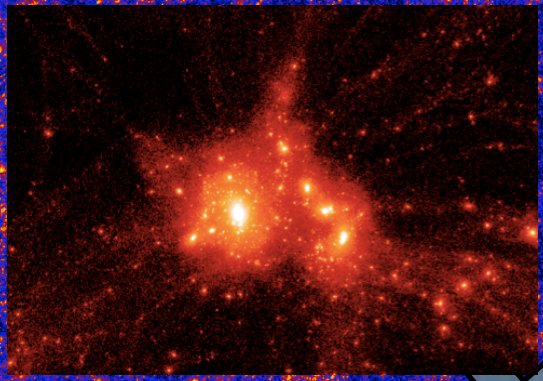


# Cold streams and hot accretion

---

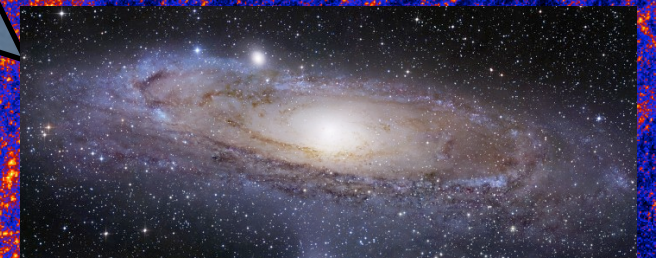
# *Galaxy Formation and Metals in The Universe*



Gas

GMC

SF



# Galaxy Formation

---

DM

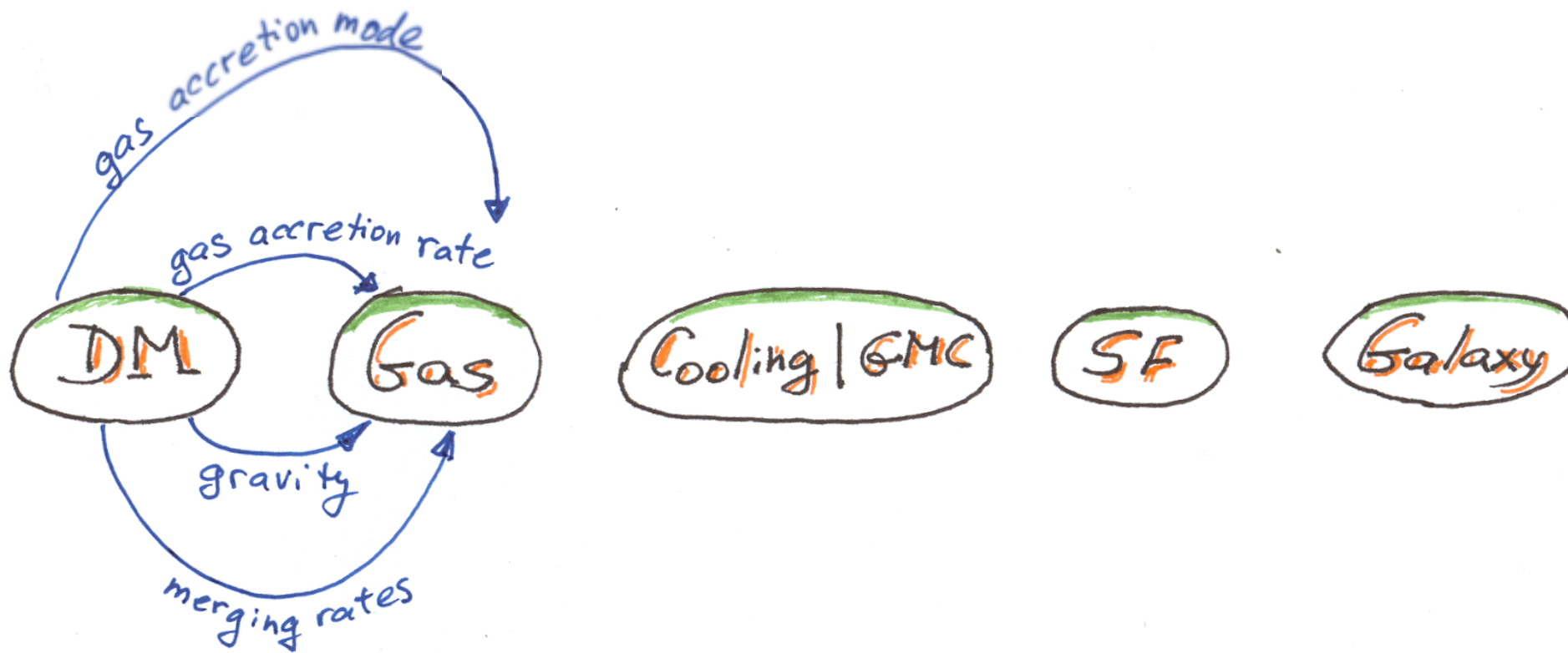
Gas

Cooling / GMC

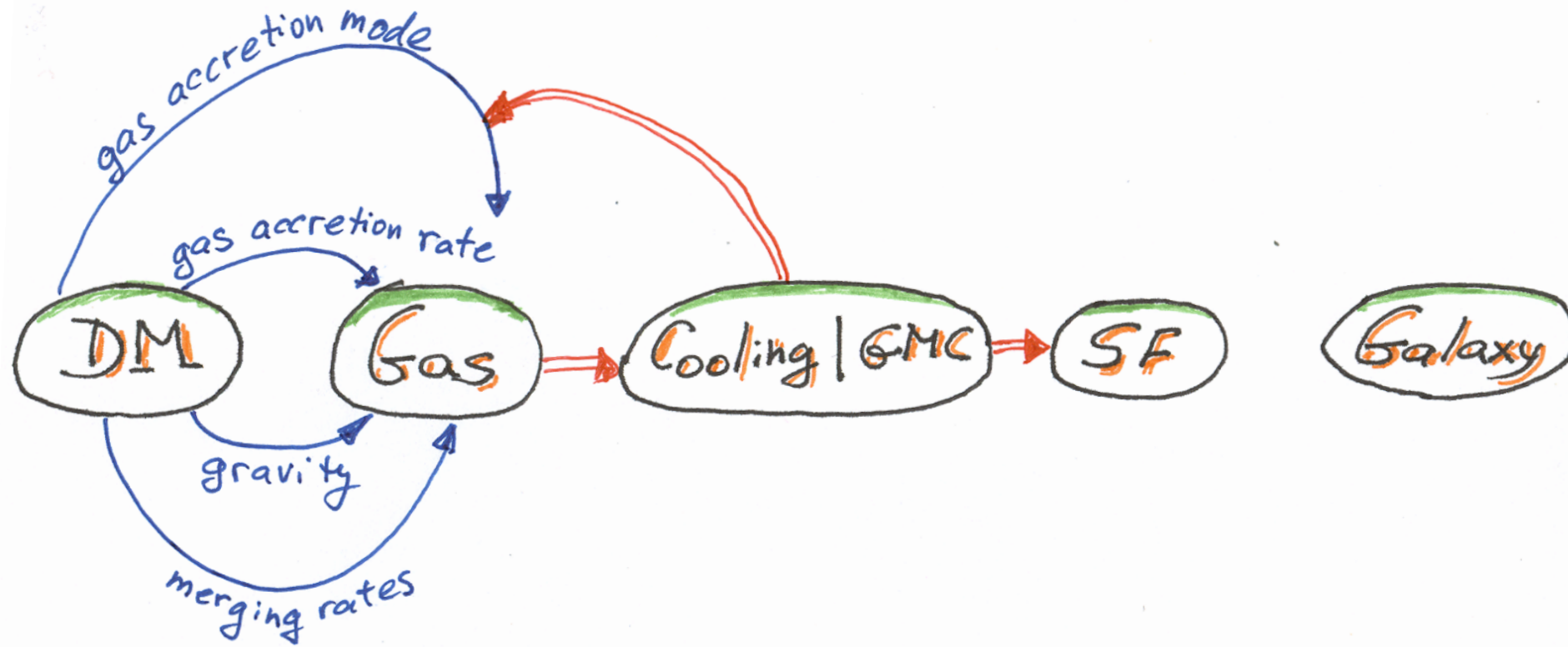
SF

Galaxy

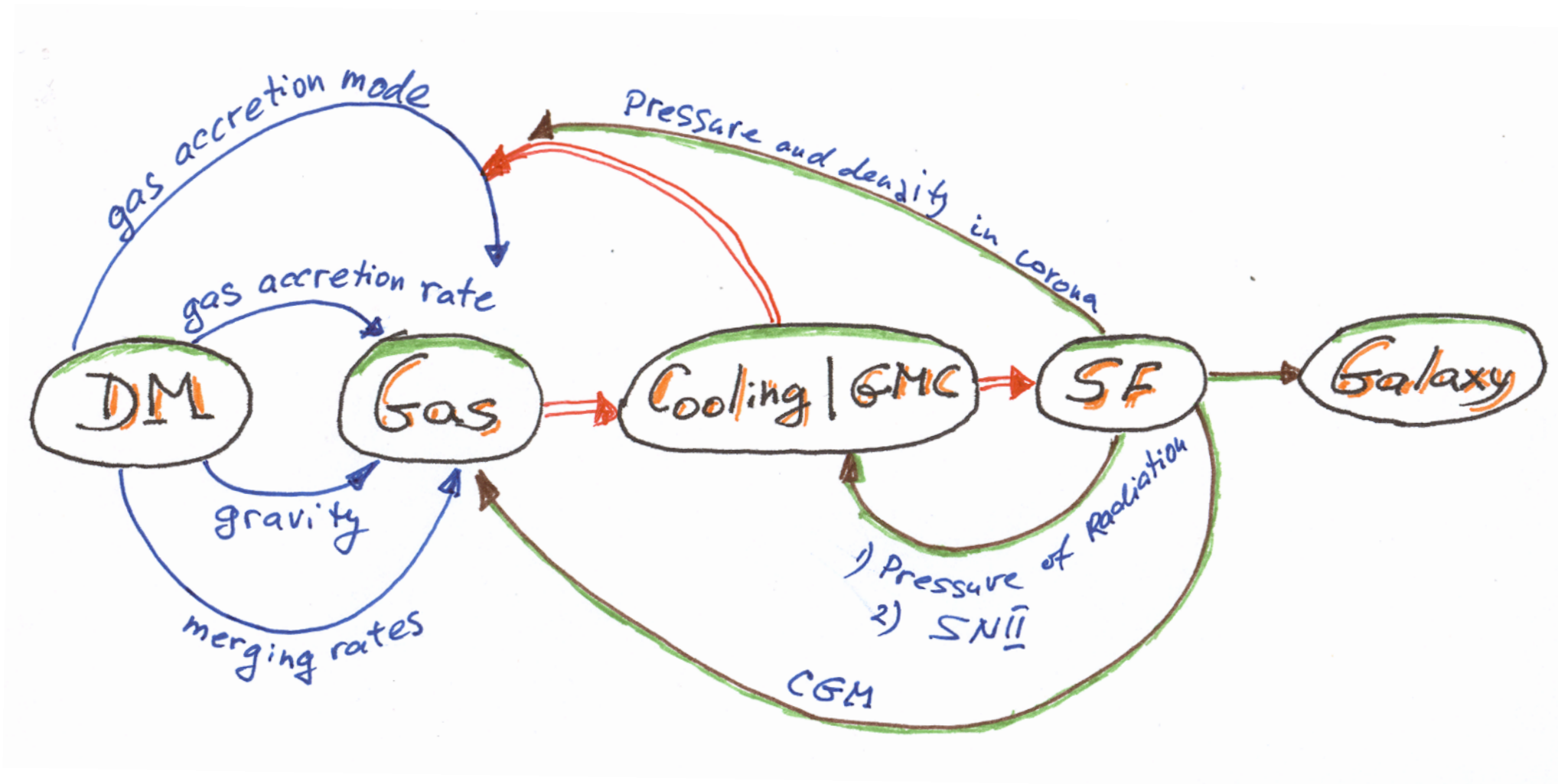
# Galaxy Formation



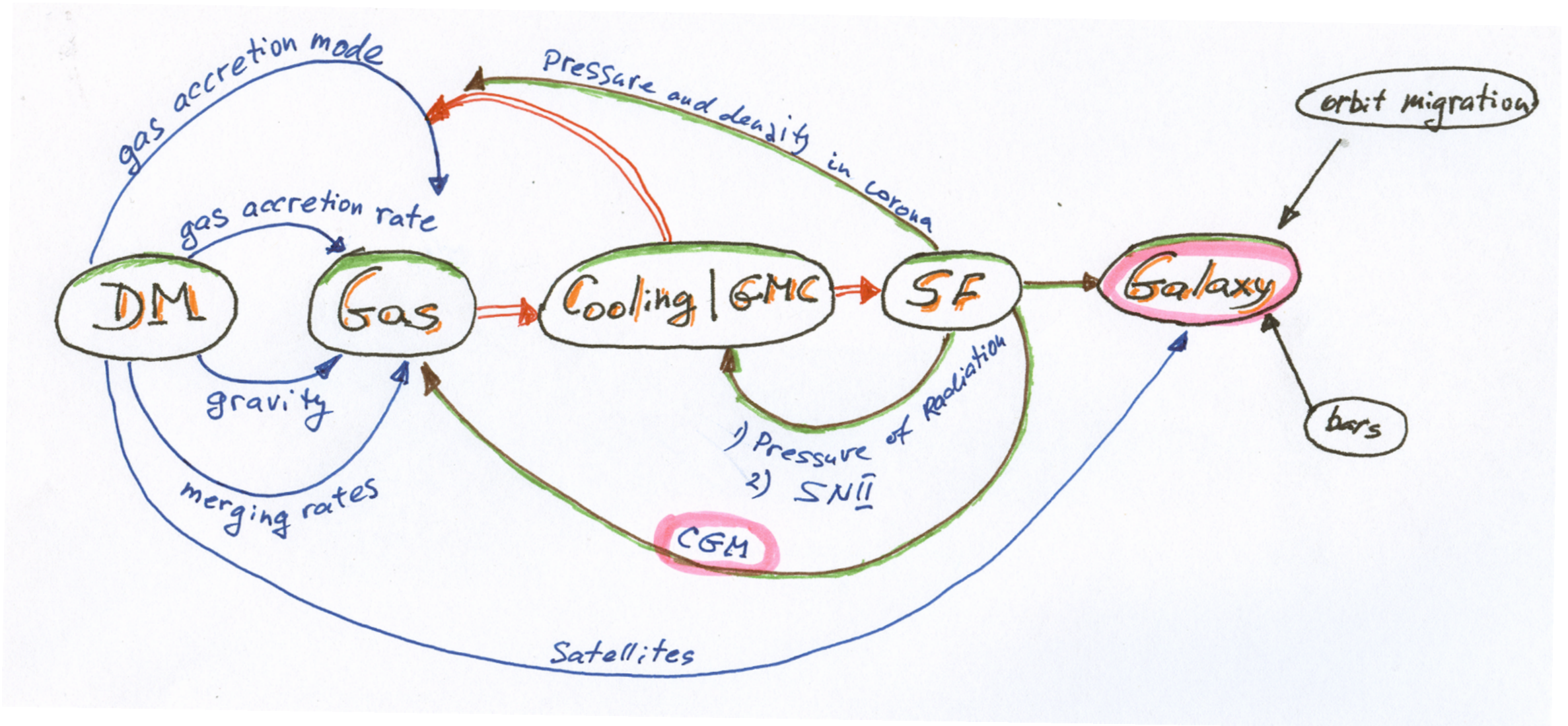
# Galaxy Formation



# Galaxy Formation

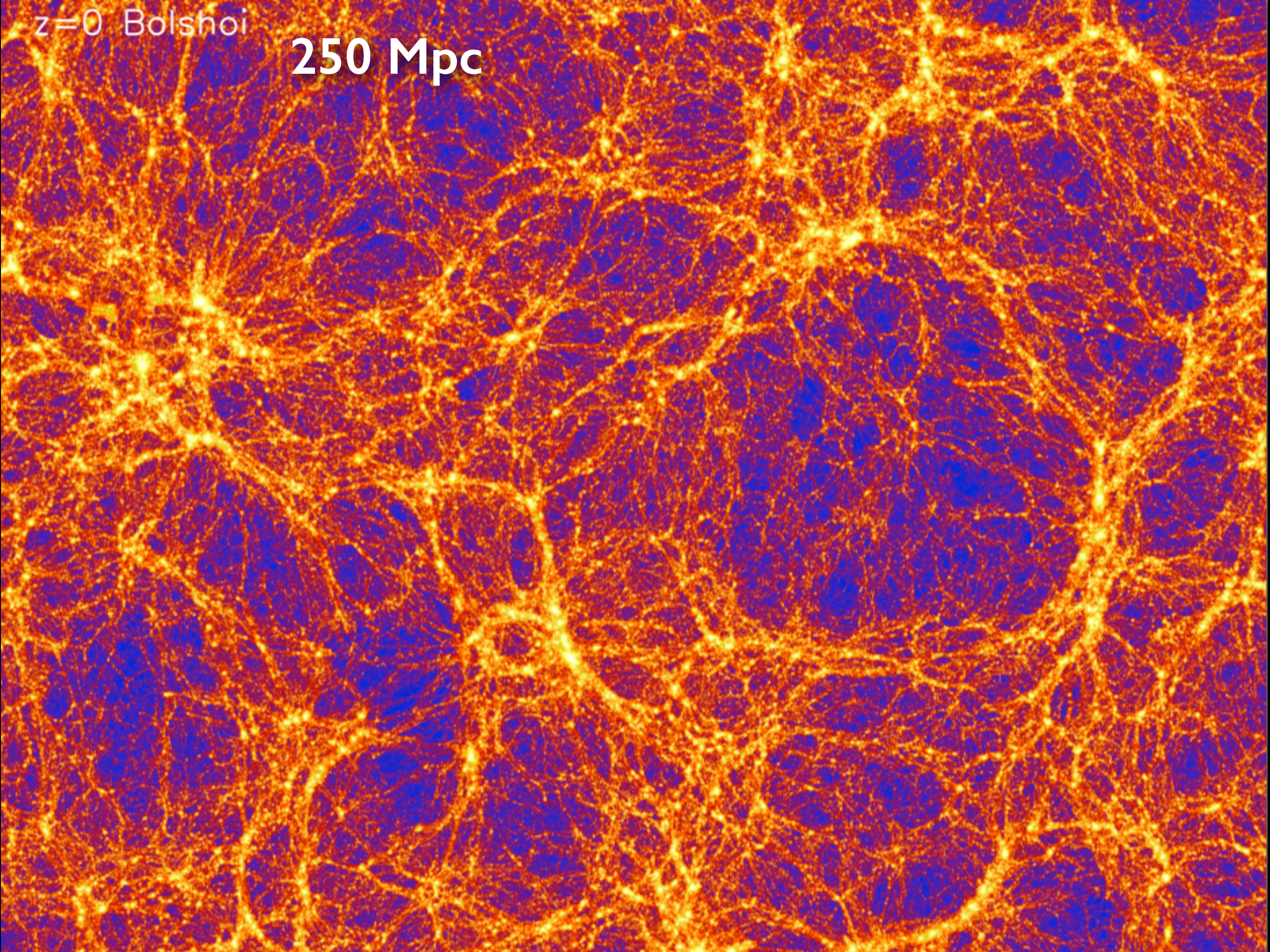


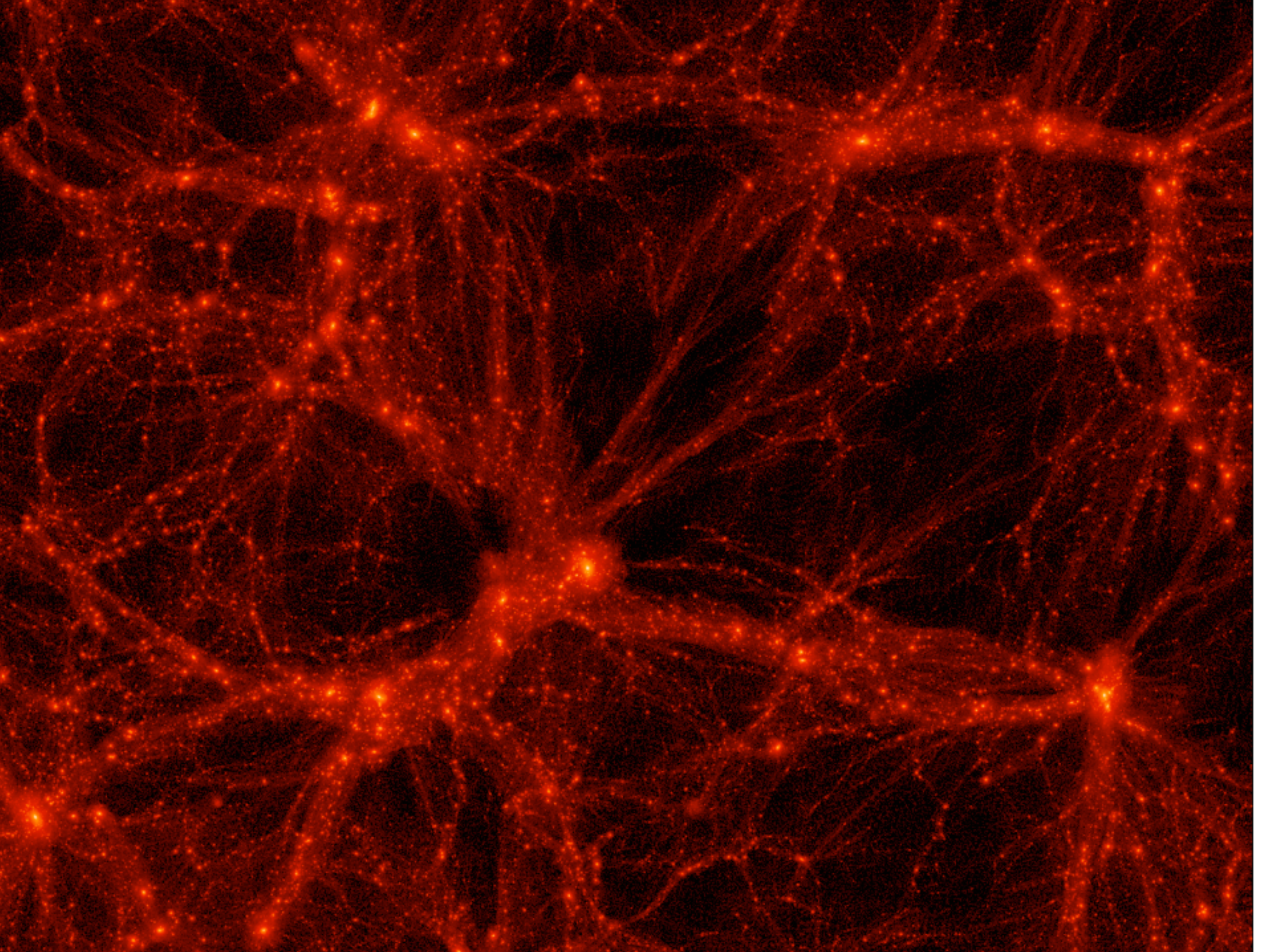
# Galaxy Formation

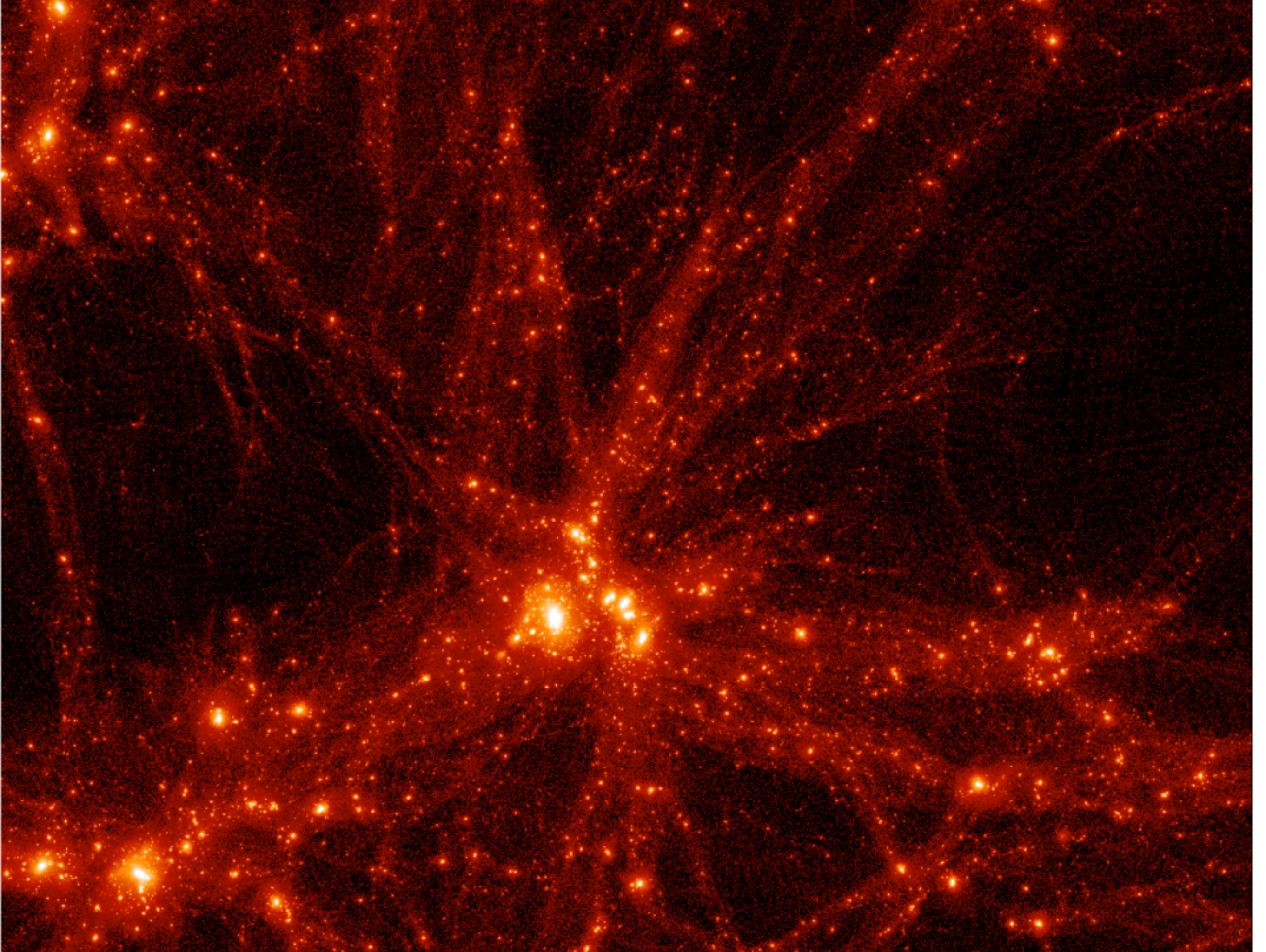


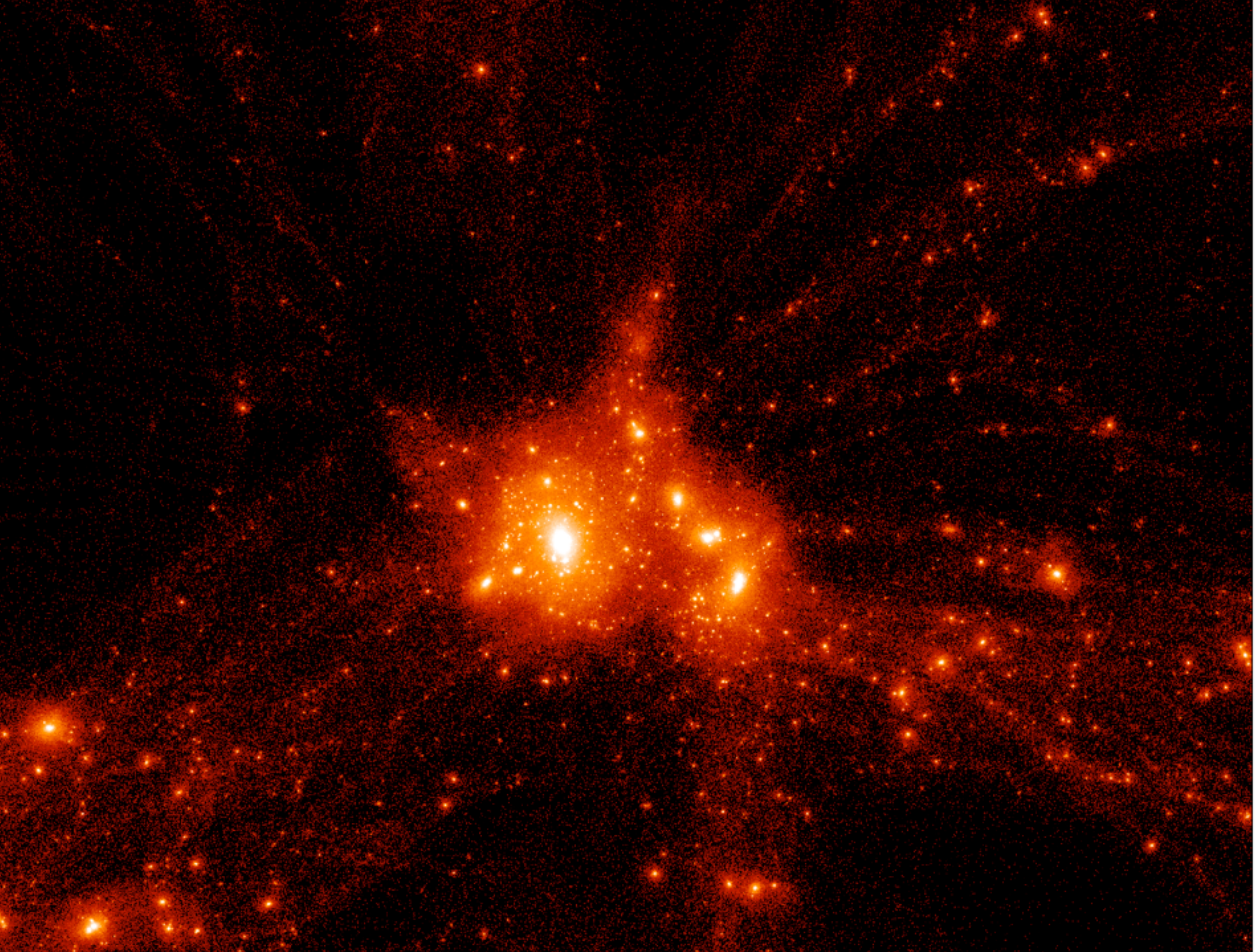
$z=0$  Bolshoi

250 Mpc



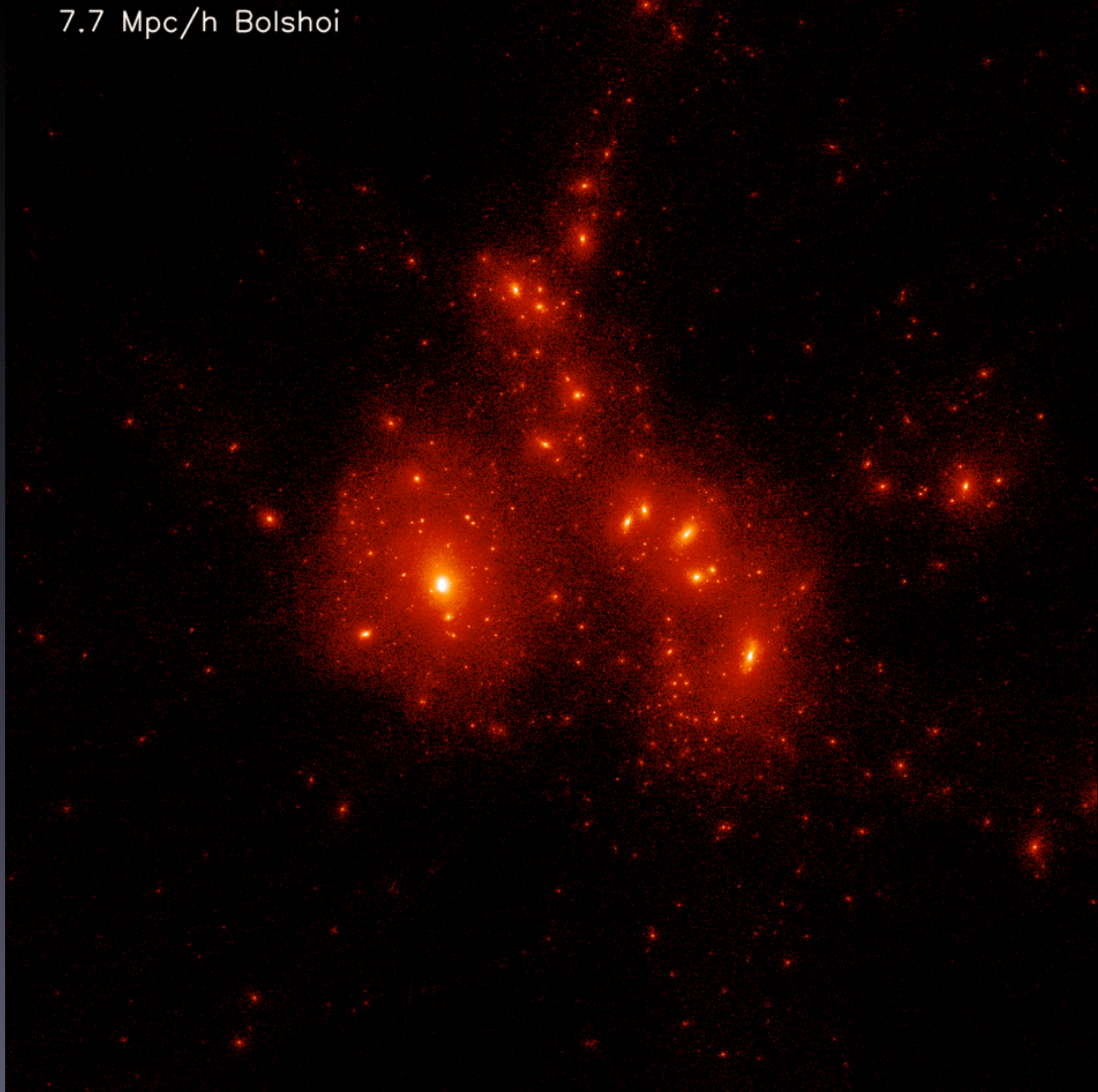




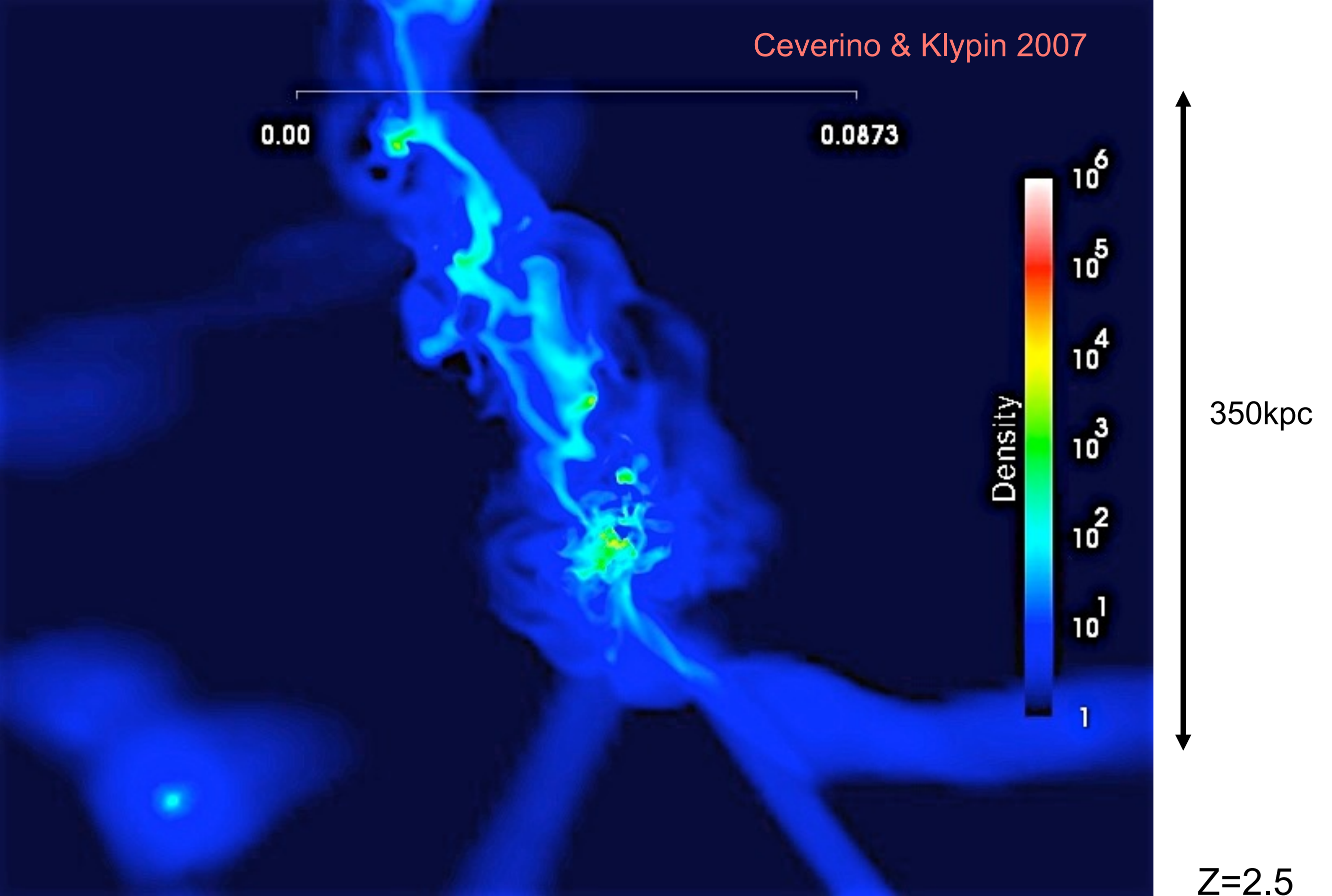


7.7 Mpc/h Bolshoi

# Small Galaxy Group



Ceverino & Klypin 2007



40pc resolution.  $M_{\text{vir}}(z=0)=1.e12M_{\text{sun}}$ .  $N_{\text{dm}}=400K$

## Virial shocks in galactic haloes? Yuval Birnboim & Avishai Dekel 2003

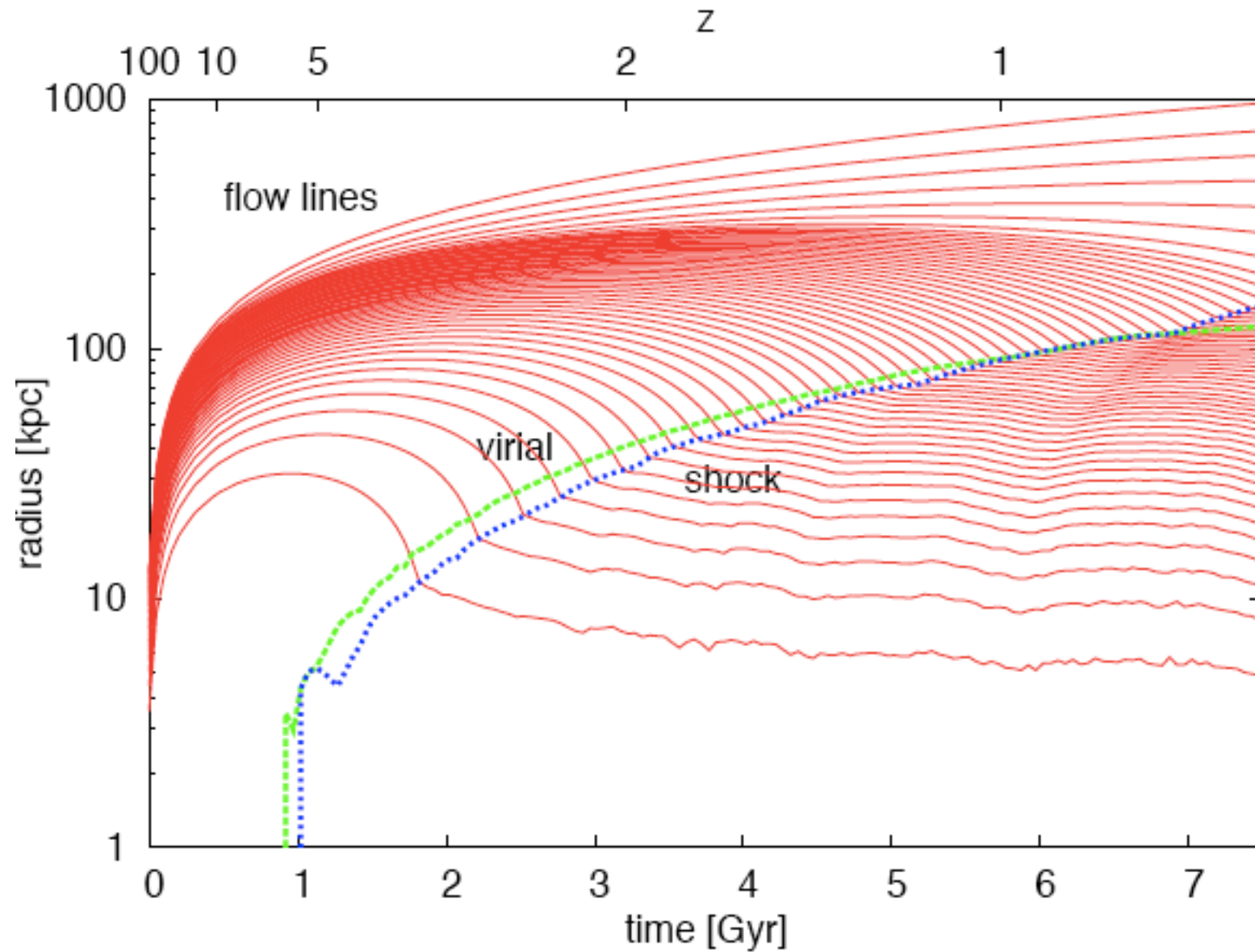
We investigate the conditions for the existence of an expanding virial shock in the gas falling within a spherical dark-matter halo. The shock relies on pressure support by the shock-heated gas behind it. When the radiative cooling is efficient compared to the infall rate the post-shock gas becomes unstable; it collapses inwards and cannot support the shock. We find for a monoatomic gas that the shock is stable when the post-shock pressure and density obey

$$\gamma_{\text{eff}} \equiv \frac{\dot{P}}{\dot{\rho}} > 10/7.$$

When the stability analysis is applied in cosmology, we find that a virial shock does not develop in most haloes that form before  $z = 2$ , and it never forms in haloes less massive than a few  $10^{11} M_{\odot}$ . In such haloes, the infalling gas is not heated to the virial temperature until it hits the disc, thus avoiding the cooling-dominated quasi-static contraction phase.

We test the validity of the shock stability criterion using numerical simulations based on a spherical hydrodynamics code which follows the evolution of shells of dark matter and gas. Since the problem we intend to examine is of global spherical symmetry, and since we need to follow the cooling and the shock with high precision, we use a one-dimensional code. Most of the simulations presented here were run using 2000 gas shells and 10,000 dark-matter shells.

The simulation starts at high redshift,  $z = 100$ , with a small spherical density perturbation. The initial density fluctuation profile is set to be proportional to the linear correlation function of the assumed cosmological model, representing the typical perturbation under the assumption that the random fluctuation field is Gaussian. The amplitude of the density fluctuation at the initial time, averaged over a given mass, determines the time of collapse, as desired. The initial velocity field is assumed to follow a quiet Hubble flow and the radial peculiar velocities build up in time.



Simulation of the *adiabatic* case. The sequence of (solid red) curves describe the log radii of Lagrangian gas shells as a function of time. The simulation was of 2000 gaseous shells (shown here) and 10,000 dark matter shells. The radius of every 20th gaseous shell is plotted. Shown on top are the virial radius and the shock. The shock exists at all times. It gradually propagates outwards, and it practically coincides with the virial radius.

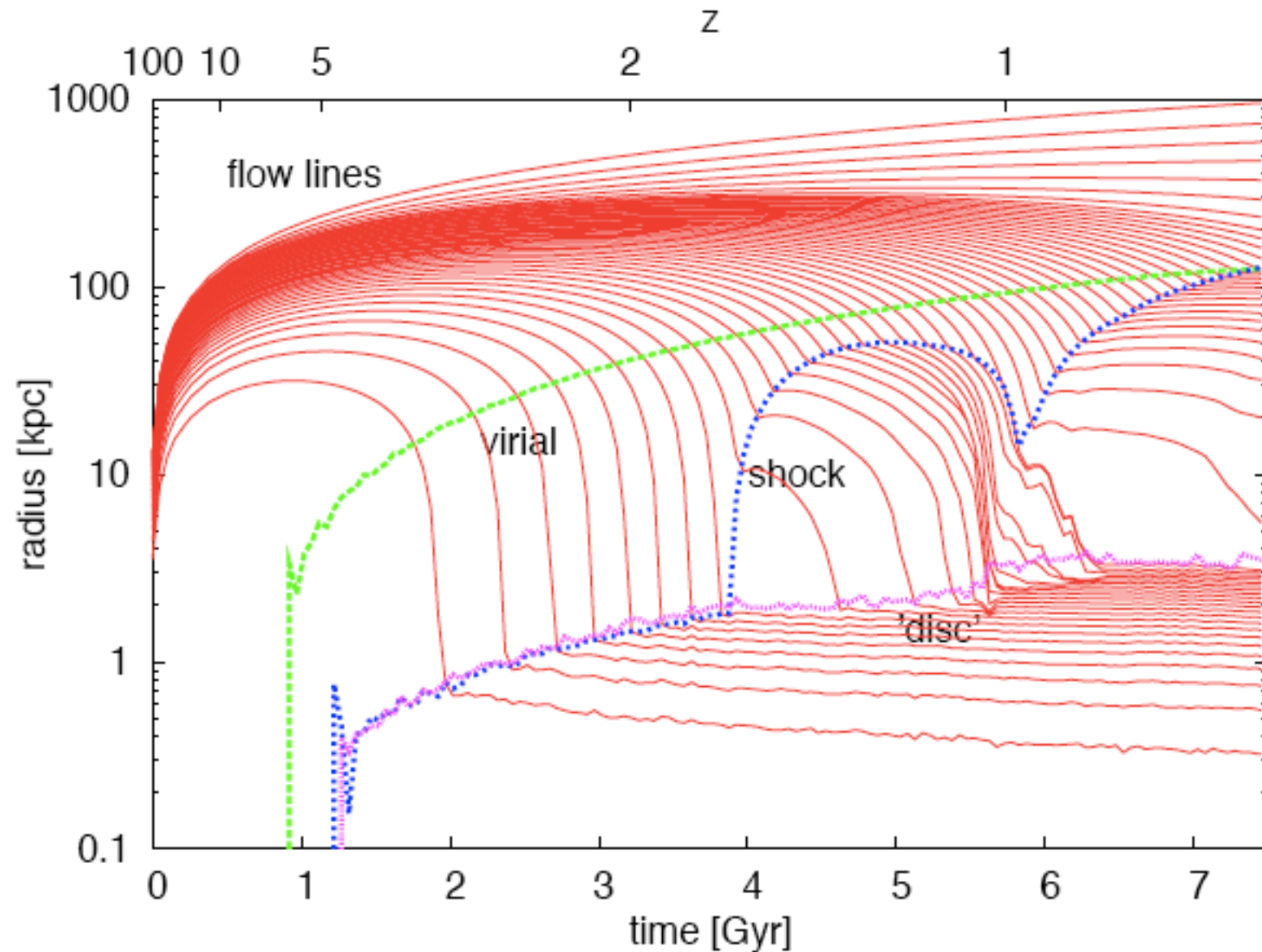


**Figure 3.** Simulation of the *radiative cooling* case, with  $Z = 0$ . The curves are as in Fig. 2, with the ‘disc’ radius added. There is no shock outside the ‘disc’ at early times, when the virial mass is small, because the cooling is too efficient. A shock develops at later times, when the mass is larger, and it quickly propagates outwards. After a couple of oscillations the shock radius approaches the virial radius.

We examine the temperature history of gas accreted by forming galaxies in smoothed particle hydrodynamics (SPH) simulations. About half of the gas follows the track expected in the conventional picture of galaxy formation, shock heating to roughly the virial temperature of the galaxy potential well ( $T \sim 10^6$  K for a Milky Way type galaxy) before cooling, condensing, and forming stars. However, the other half radiates its acquired gravitational energy at much lower temperatures, typically  $T < 10^5$  K, and the histogram of maximum gas temperatures is clearly bimodal. The “cold mode” of gas accretion dominates for low mass galaxies (baryonic mass  $M_{\text{gal}} \lesssim 10^{10.3} M_{\odot}$  or halo mass  $M_{\text{halo}} \lesssim 10^{11.4} M_{\odot}$ ), while the conventional “hot mode” dominates the growth of high mass systems. Cold accretion is often directed along filaments, allowing galaxies to efficiently draw gas from large distances, while hot accretion is quasi-spherical. The galaxy and halo mass dependence leads to redshift and environment dependence of cold and hot accretion rates, with cold mode dominating at high redshift and in low density regions today, and hot mode dominating in group and cluster environments at low redshift. The simulations reproduce an important feature of the observed relation

Our primary results are derived from a simulation that models a  $22.222h^{-1}$  Mpc comoving periodic cube using  $128^3$  dark matter particles and  $128^3$  gas particles. Gravitational forces are softened using a cubic spline kernel of comoving radius  $5h^{-1}$  kpc, approximately equivalent to a Plummer force softening of  $\epsilon_{\text{grav}} = 3.5h^{-1}$  kpc. Our baryonic mass threshold for resolved galaxies (see §2.3) is  $6.8 \times 10^9 M_{\odot}$ , the mass of 64 gas particles, and there are 1120 galaxies in the box above this threshold at  $z = 0$ . To approximately match

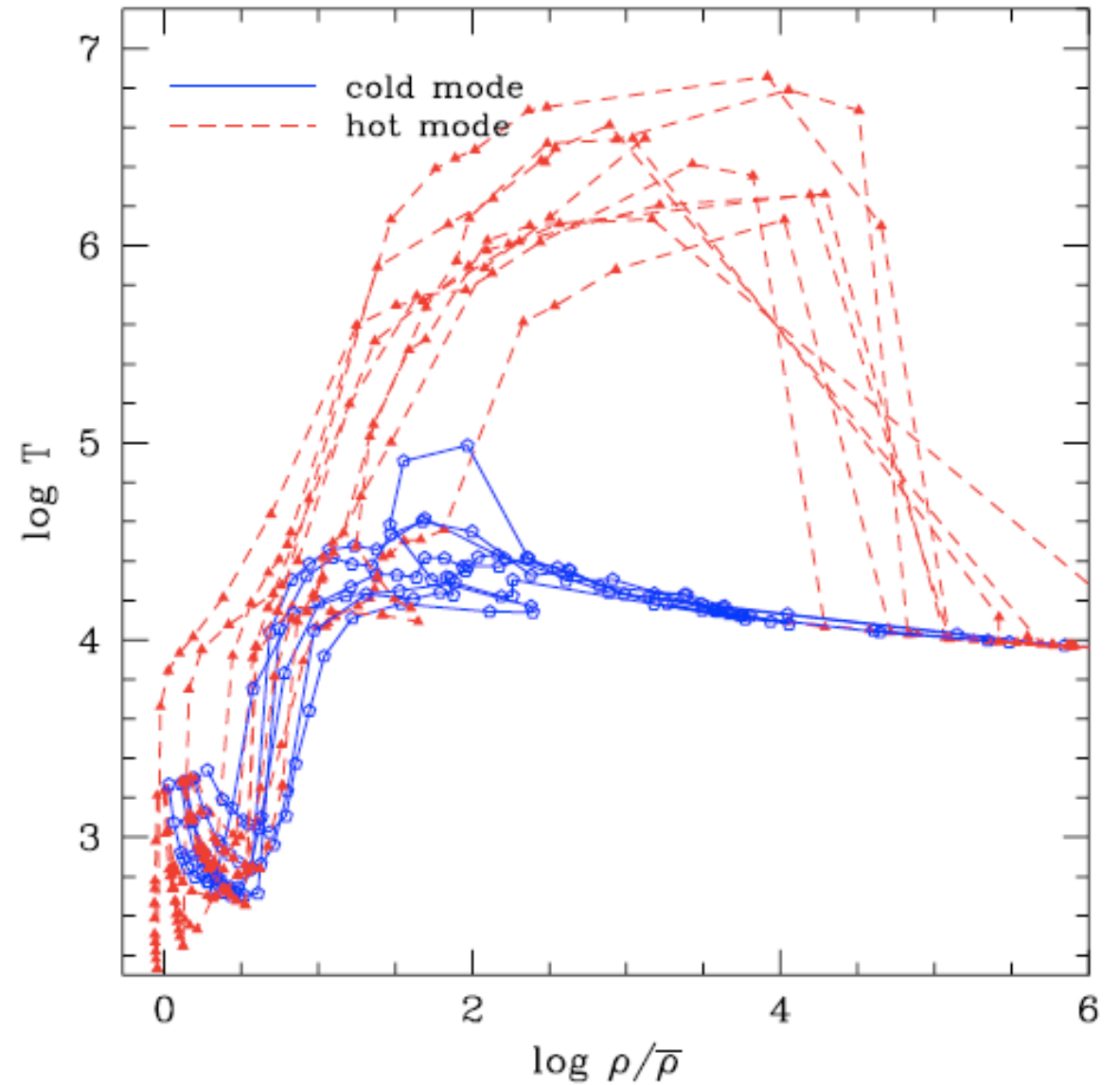
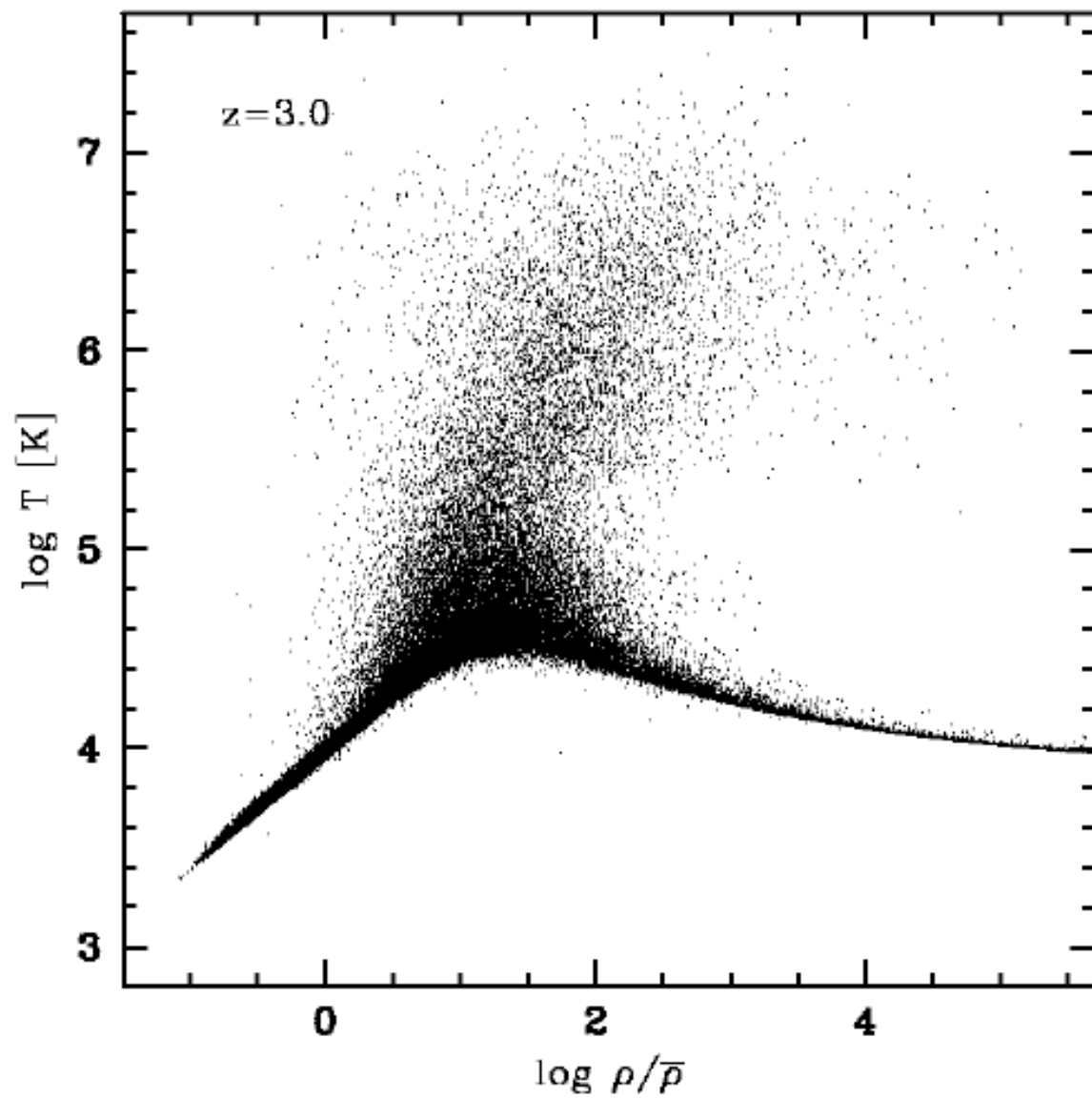
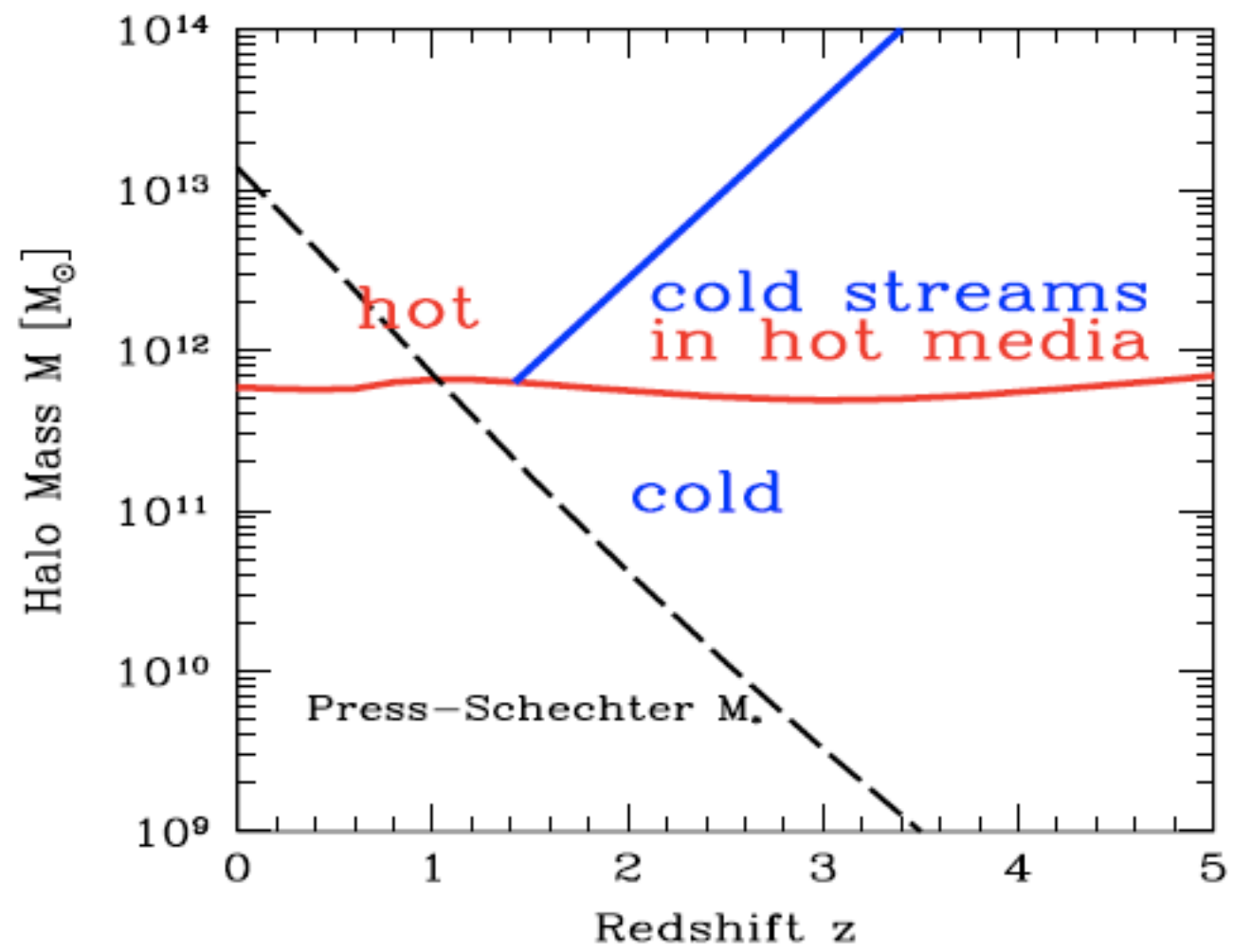


**Figure 1.** *Left:* Distribution of gas particles in the  $\rho - T$  plane at  $z = 3$ , in the L22/128 simulation. One can easily identify three major phases: low density, low temperature gas in the photoionized IGM, shock heated overdense gas, and high density, radiatively cooled gas within galaxies. *Right:* Trajectories of 15 particles that accreted onto galaxies shortly before  $z = 3$ , illustrating the “cold” (solid lines, circles) and “hot” (dashed lines, triangles) accretion modes. Hot mode particles are shock heated above  $\sim 10^{5.5}$  K before cooling, while cold mode particles move directly from the diffuse IGM phase to the dense, galactic phase without ever heating above  $10^5$  K. Trajectories start at  $z = 14.9$  and end at  $z = 3$ . Points mark the individual redshift outputs, which have typical time separations of 0.05-0.1 Gyr.



# Cold streams in early massive hot haloes as the main mode of galaxy formation. Dekel et al 2009, Nature

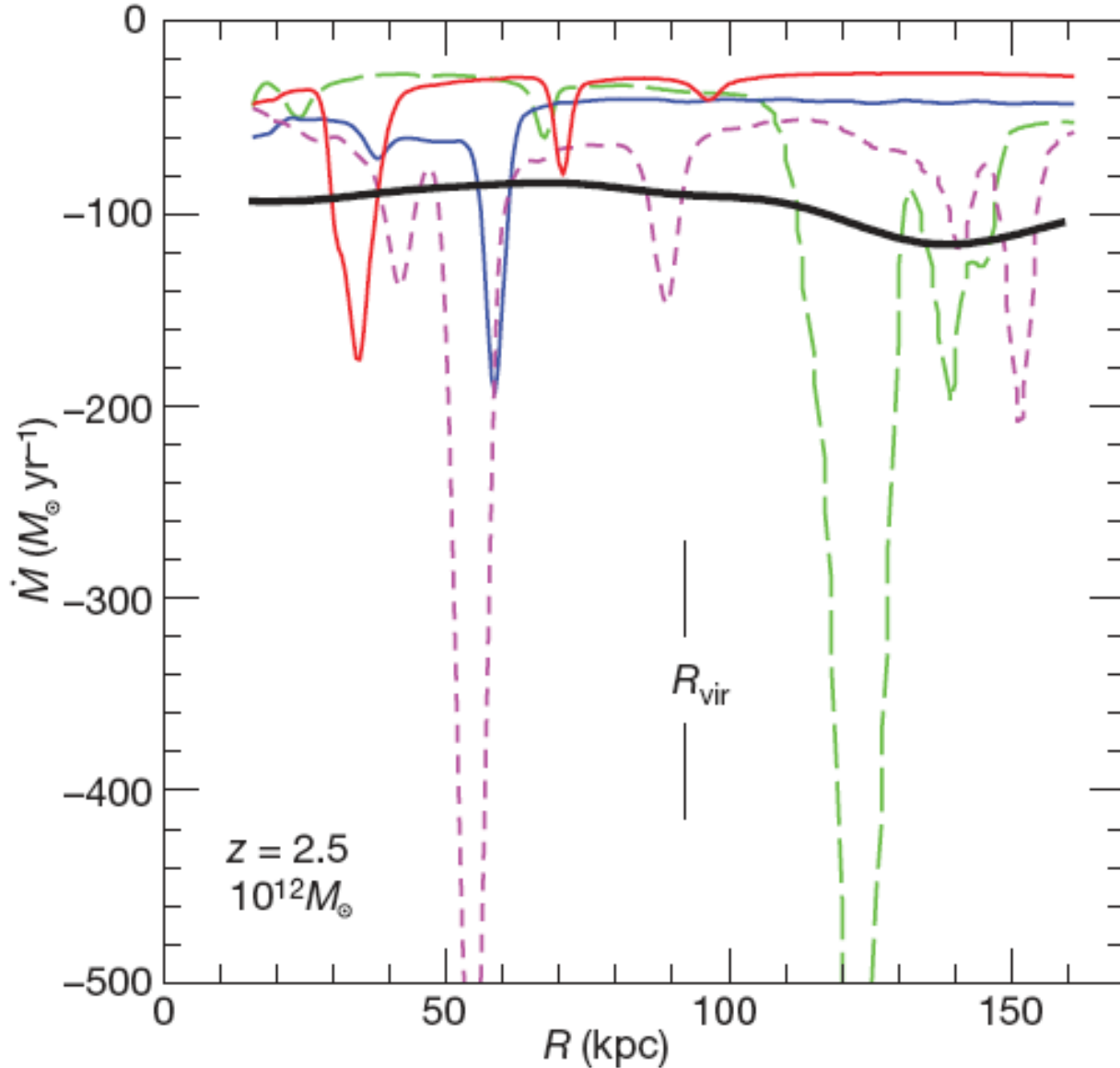
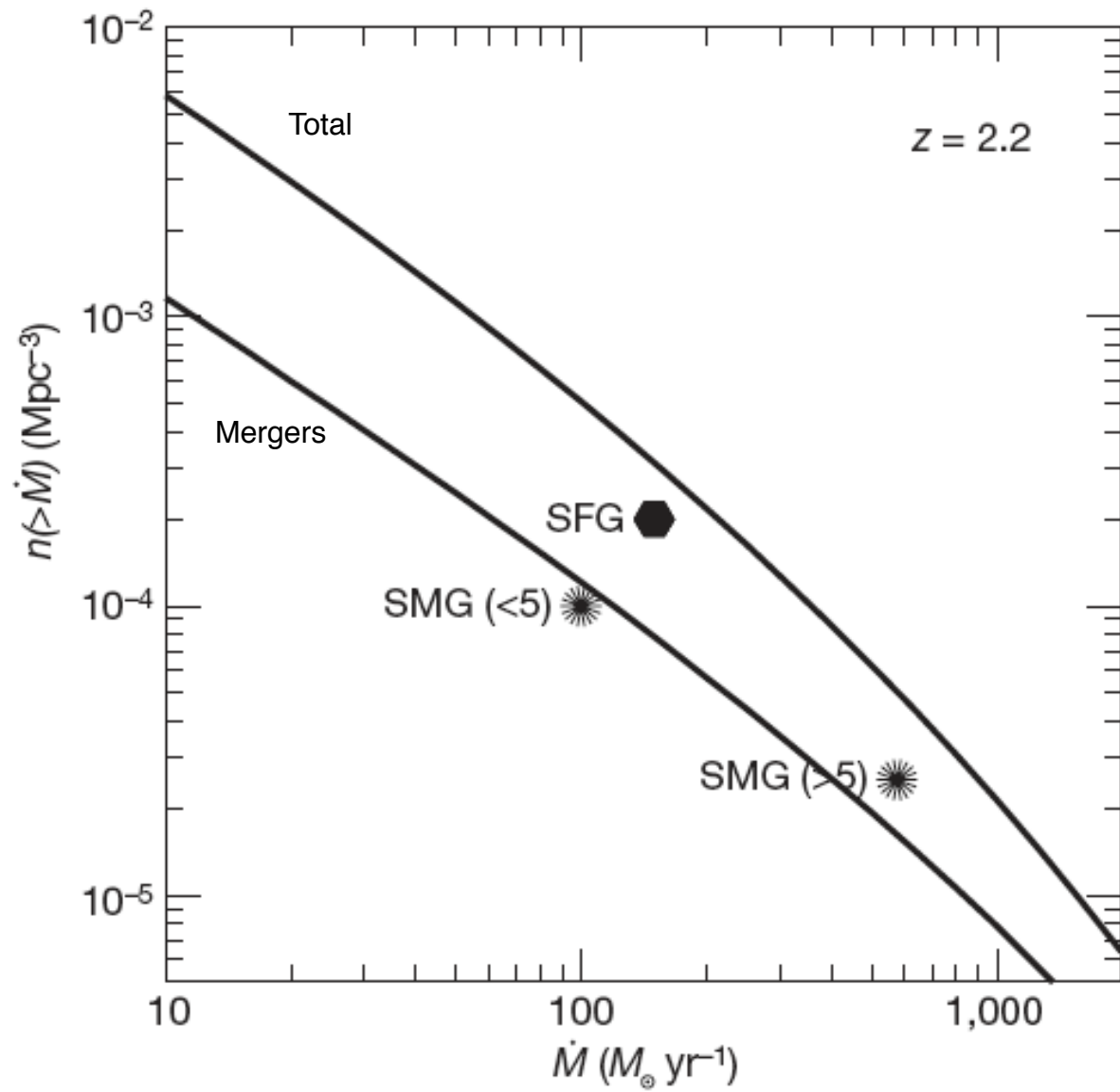


**Figure 3 | Accretion profiles,  $\dot{M}(r)$ .** Shown is the gas inflow rate through spherical shells of radius  $r$ , from the disk vicinity to almost twice the halo virial radius, obtained by integrating  $r^2 \rho v_r$  over the whole shell. The thick black curve is the average over the simulated galaxies of the fiducial case,  $M_v \approx 10^{12} M_\odot$  at  $z = 2.5$ . It shows deep penetration at a roughly constant rate of  $\sim 100 M_\odot \text{ yr}^{-1}$ , consistent with the virial growth rate predicted by equation (1). Apparently, the inflow rate does decay as the gas travels through the halo, but this decay is roughly compensated for by the higher cosmological inflow rate when that gas entered the halo (equation (1)), leading to the apparent constancy of accretion rate with radius. The coloured curves refer to four representative galaxies, two showing clumps with  $\mu \gtrsim 0.1$  (dashed lines) and two with smoother flows involving only minor clumps with  $\mu < 0.1$  (solid lines). Clumps with  $\mu \gtrsim 0.3$  appear within  $2R_v$  about once in every ten galaxies; that is, major mergers are infrequent (Supplementary Fig. 7). The  $\dot{M}(r)$  profiles serve for extracting the conditional probability distribution  $P(\dot{M} | M_v)$ , leading to the abundance  $n(>\dot{M})$  (Supplementary Fig. 8).

The average growth rate of halo mass,  $M_v$ , through mergers and smooth accretion, is derived<sup>6</sup> on the basis of the extended Press-Schechter (EPS) theory of gravitational clustering (Supplementary Information, section 1) or from cosmological simulations<sup>16, 17</sup>. For  $\Lambda$ CDM, the corresponding growth rate of the baryonic component is approximately

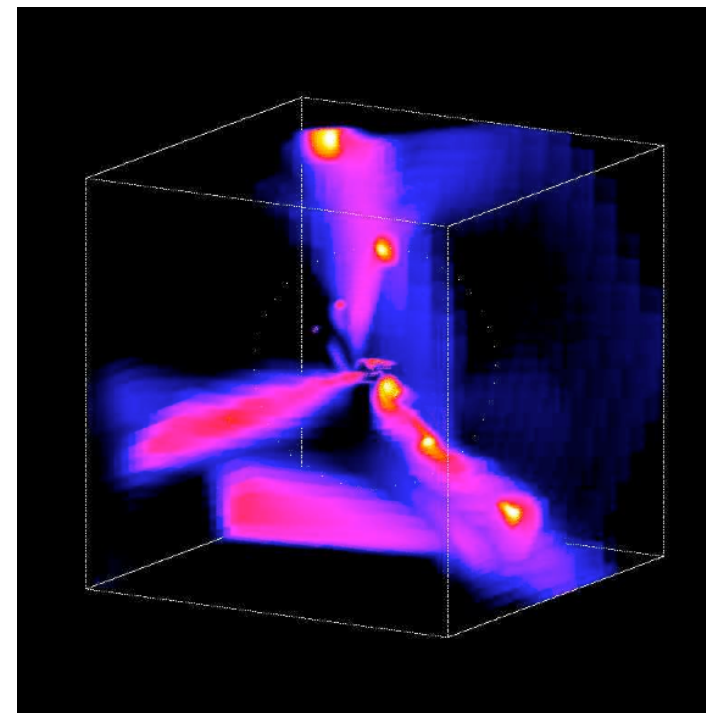
$$\dot{M} \approx 6.6 M_{12}^{1.15} (1+z)^{2.25} f_{0.165} M_\odot \text{ yr}^{-1} \quad (1)$$

where  $M_{12} \equiv M_v / 10^{12} M_\odot$  and  $f_{0.165}$  is the baryonic fraction in the haloes in units of the cosmological value,  $f_b = 0.165$ . Thus, at  $z = 2.2$ , the baryonic growth rate of haloes of mass  $2 \times 10^{12} M_\odot$  is  $\dot{M} \approx 200 M_\odot \text{ yr}^{-1}$ , sufficient to maintain the SFR in SFGs. However, the margin by

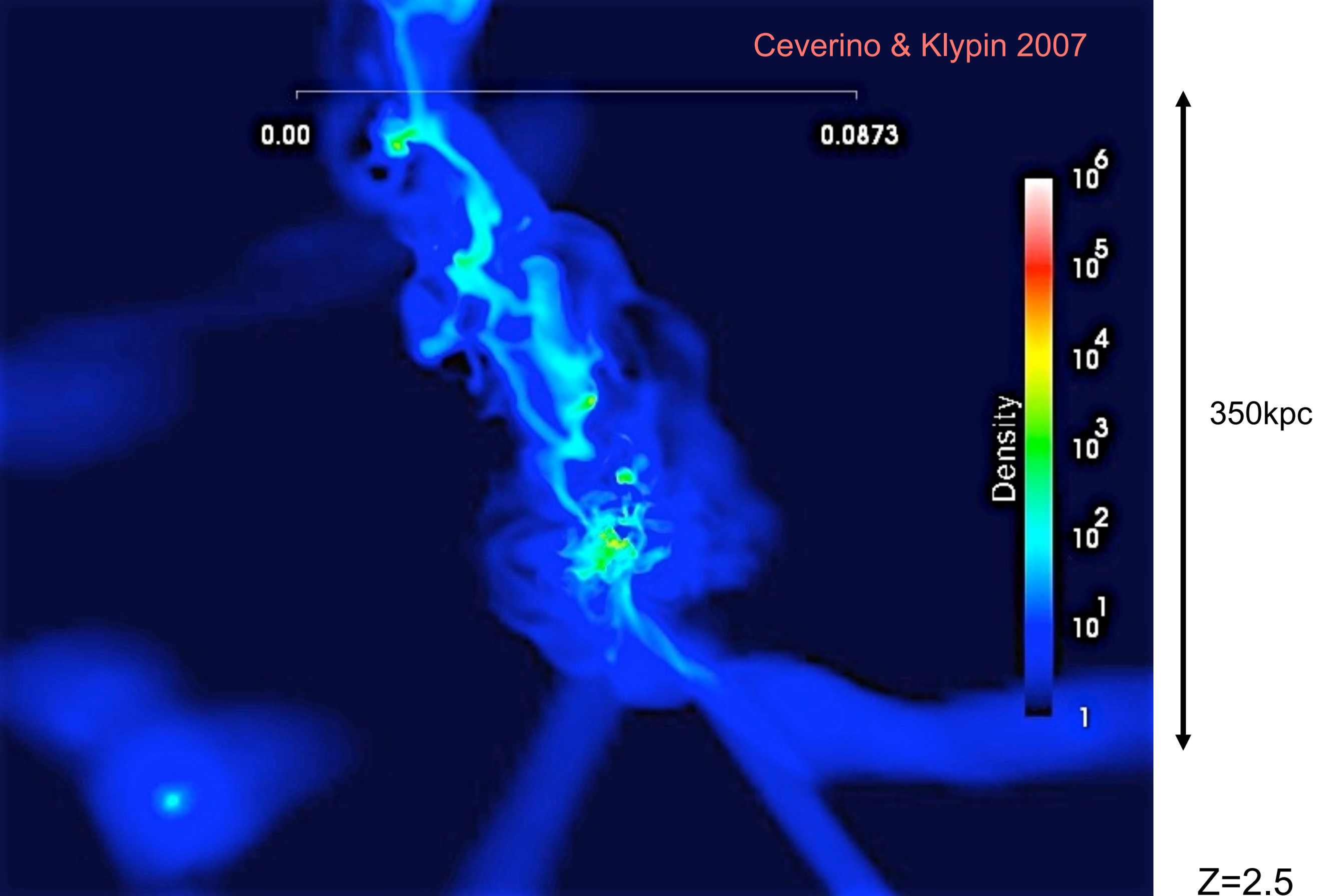


SFG - star forming galaxies (UV-selected)  $n = 2 \times 10^{-4} \text{ Mpc}^{-3}$   $M_{\text{vir}} = 3.5 \times 10^{12} M_{\odot}$   
 SMG- Sub-Millimeter Galaxies, dusty,  $n = 2 \times 10^{-5} \text{ Mpc}^{-3}$

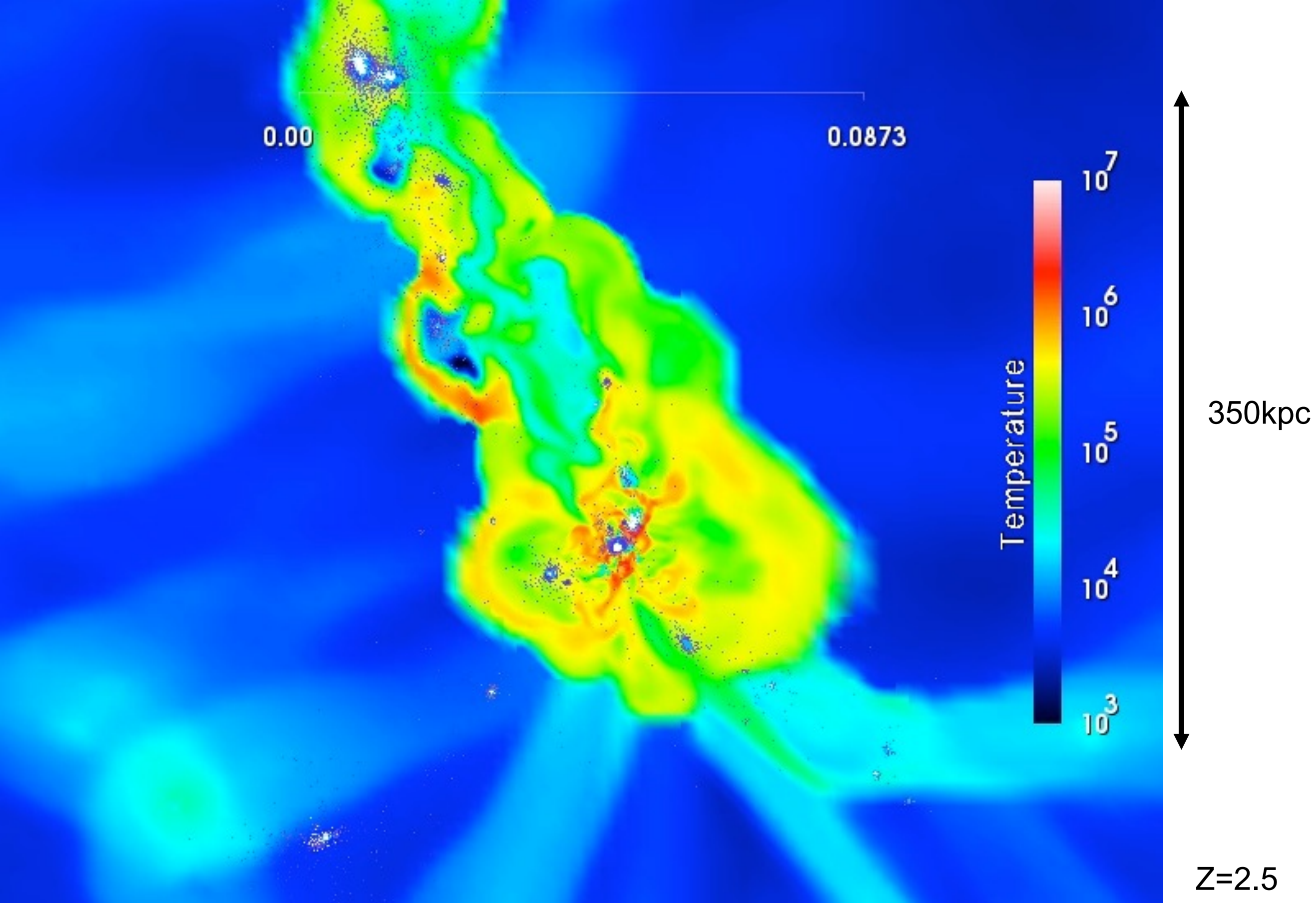
**Figure 4 | Abundance of galaxies as a function of gas inflow rate,  $n(>\dot{M})$ .** Shown is the co-moving number density,  $n$ , of galaxies with inflow rate higher than  $\dot{M}$  at  $z = 2.2$ , as predicted from our analysis of the cosmological simulation. The upper curve refers to total inflow. It shows that galaxies with  $\dot{M} > 150 M_{\odot} \text{ yr}^{-1}$  are expected at a co-moving number density  $n \approx 3 \times 10^{-4} \text{ Mpc}^{-3}$  (similar to estimates in other simulations<sup>32,33</sup>). Fluxes as high as  $\dot{M} > 500 M_{\odot} \text{ yr}^{-1}$  are anticipated at  $n \approx 6 \times 10^{-5} \text{ Mpc}^{-3}$ . The lower curve is similar, but limited to gas input by  $\mu > 0.1$  mergers. The symbols represent the vicinity of where the observed massive star-forming galaxies can be located once their observed SFRs are identified with  $\dot{M}$ . The sBzK and BX/BM galaxies are marked SFG<sup>13</sup>. The SMGs respectively brighter and fainter than 5 mJy are marked accordingly<sup>12,13</sup>. We see that the overall gas inflow rate is sufficient for the observed SFR, but the small margin implies that the SFR must closely follow the rate of gas supply. Most of the massive star formers at a given SFR are expected to be observed while being fed by smooth flows rather than undergoing mergers. By studying the contribution of different halo masses to the abundance  $n(>\dot{M})$ , we learn that the high-SFR SFGs and SMGs are associated with haloes of mass  $10^{12} M_{\odot} - 10^{13} M_{\odot}$  (Supplementary Fig. 9). An integration of  $\dot{M}$  over halo mass and time reveals that most of the stars in the universe were formed in stream-fed galaxies, within haloes of mass  $> 2 \times 10^{11} M_{\odot}$  at  $1.5 < z < 4$ .



Ceverino & Klypin 2007



40pc resolution.  $M_{\text{vir}}(z=0)=1.e12M_{\text{sun}}$ .  $N_{\text{dm}}=400K$



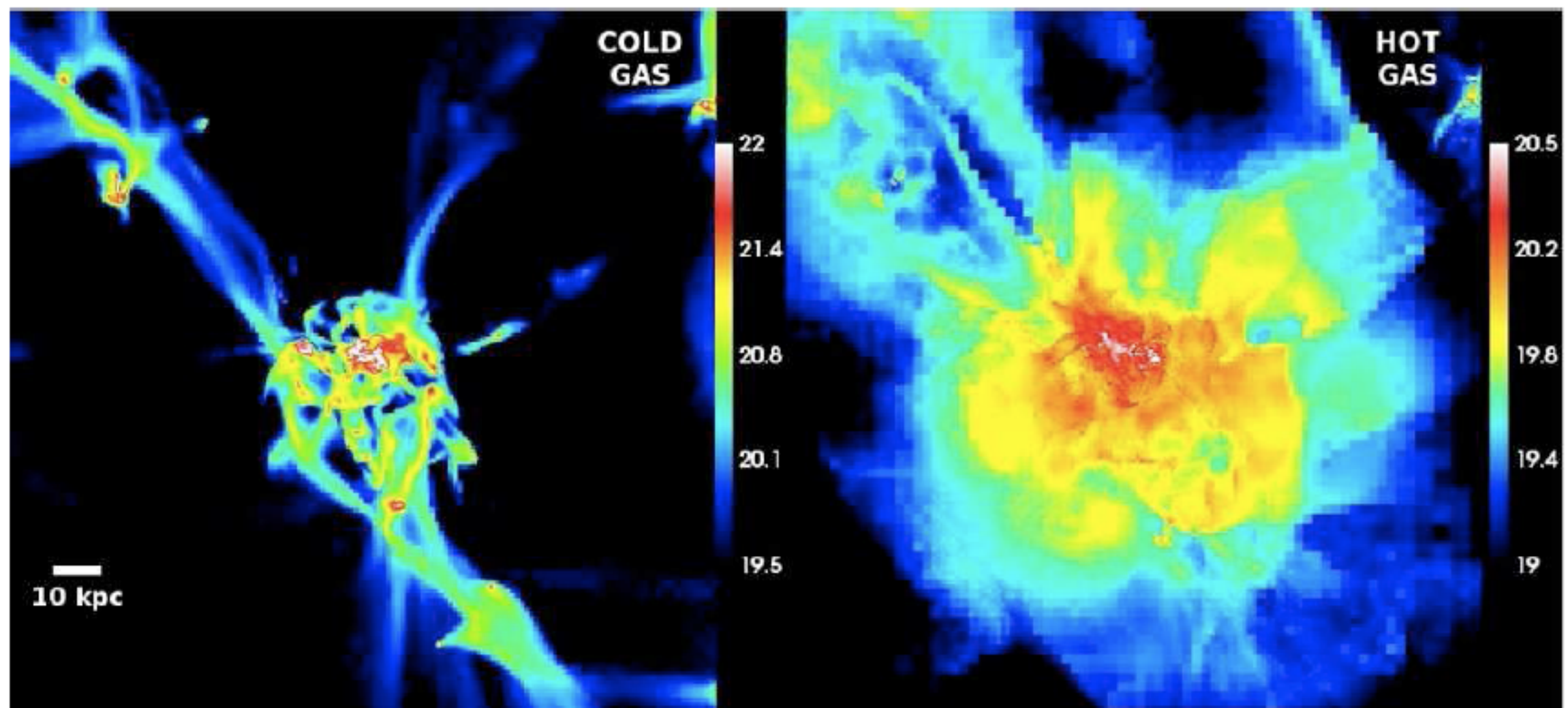
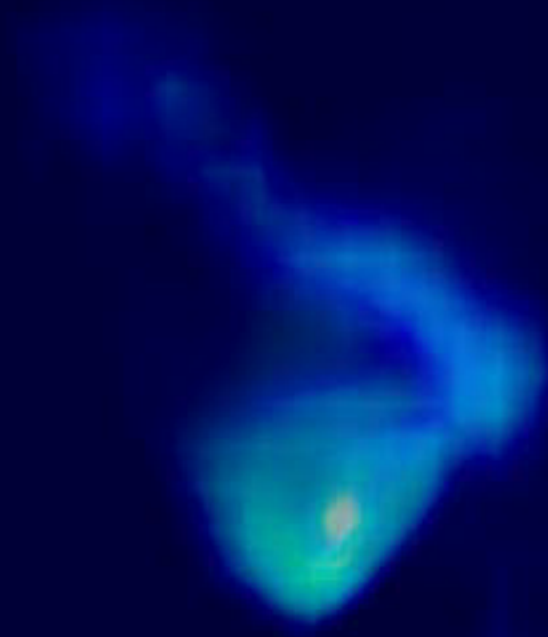
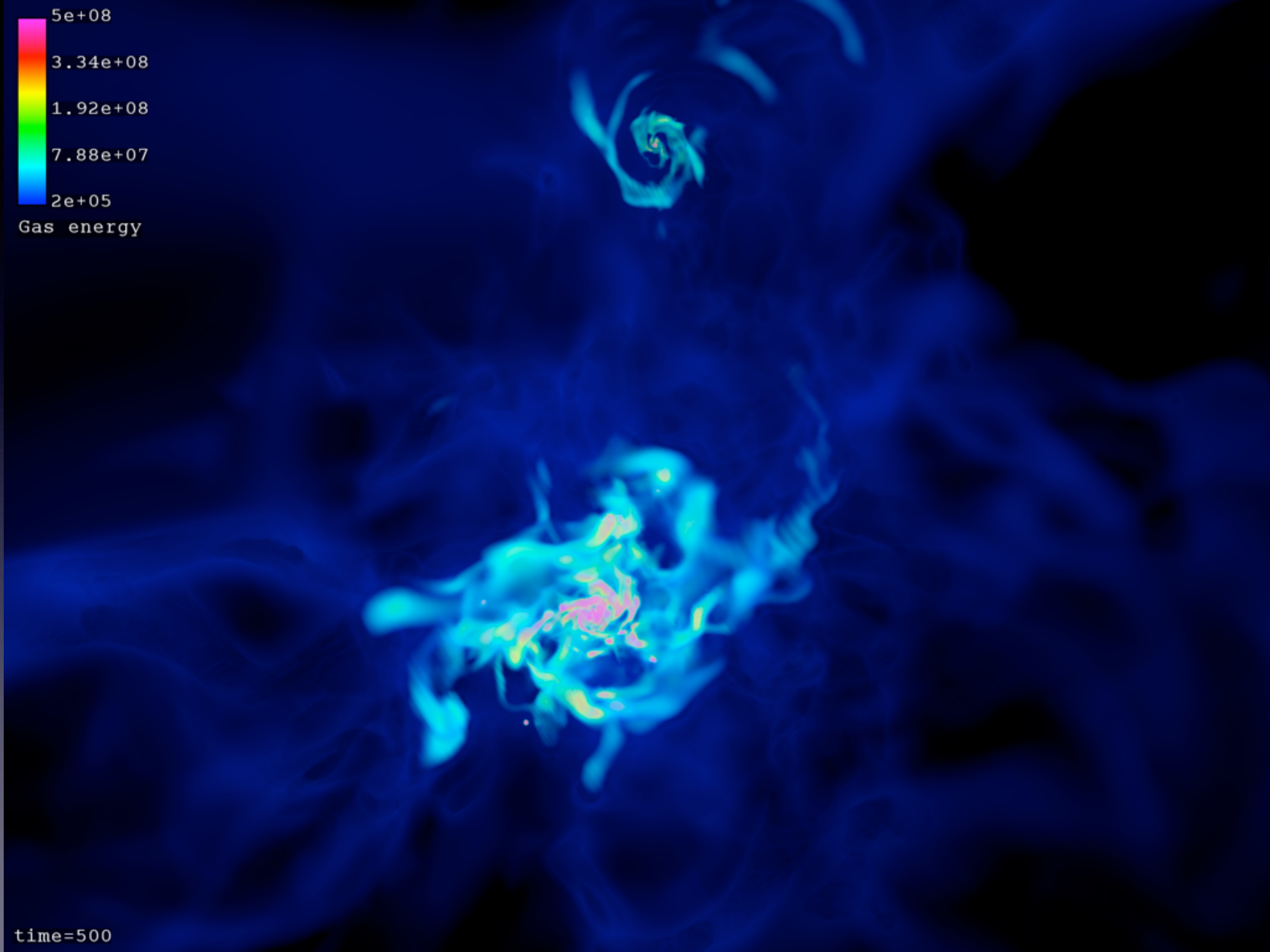


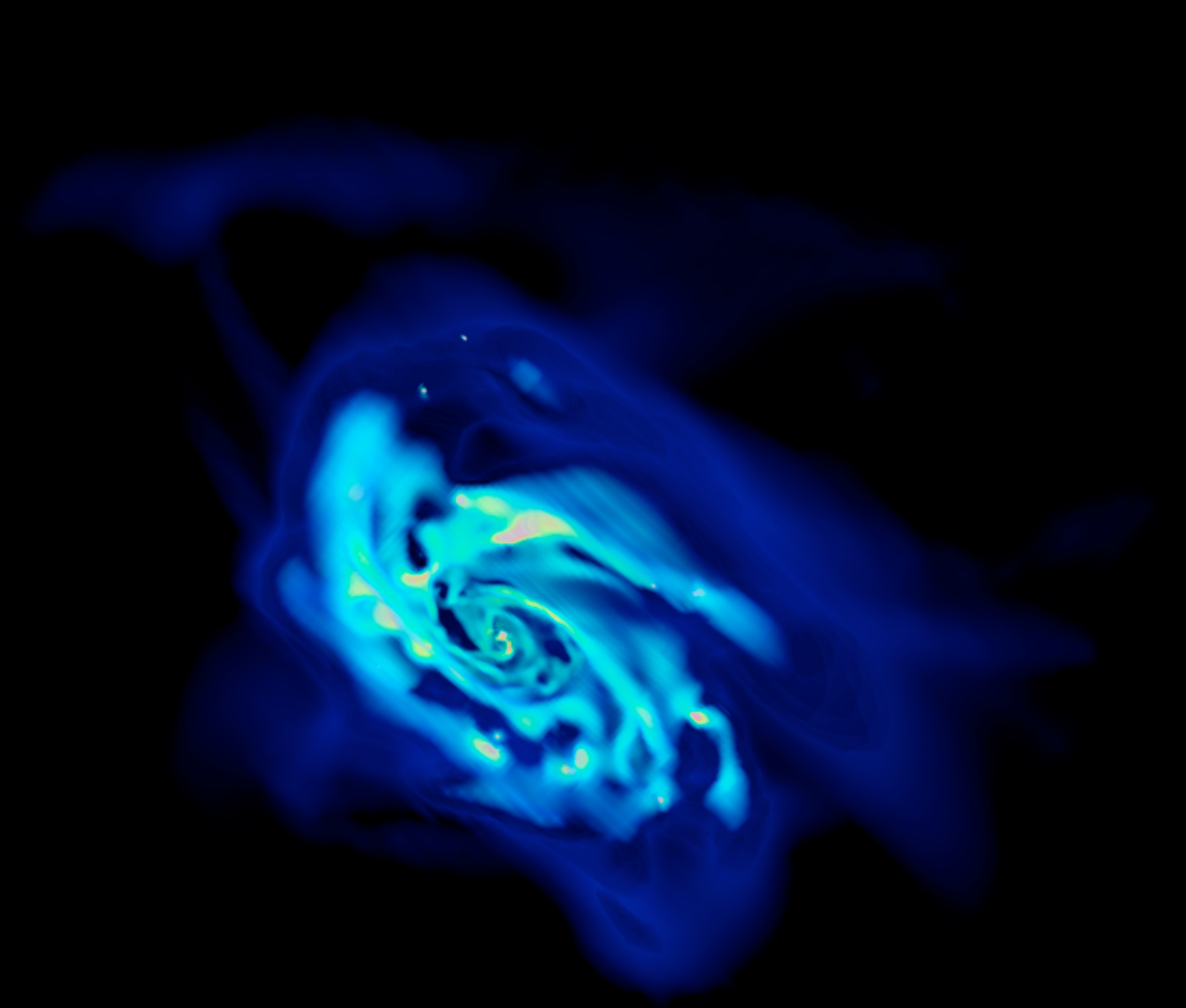
Figure 3. A zoom-out gas surface-density maps showing the streams feeding galaxy A. Left: cold gas ( $T < 5 \times 10^4$  K). Right: hot gas ( $T > 3 \times 10^5$  K). The box size is  $160 \times 160$  kpc, covering the whole virial sphere. The color refers to log gas surface density in units of H atoms  $\text{cm}^{-2}$ . Two major narrow streams carry the gas from well outside the virial radius to the inner  $\sim 20$  kpc halo core, where they break into a multi-stream turbulent core before joining the inner disc of radius  $\sim 6$  kpc, seen nearly edge-on at the box centre (mostly in white).



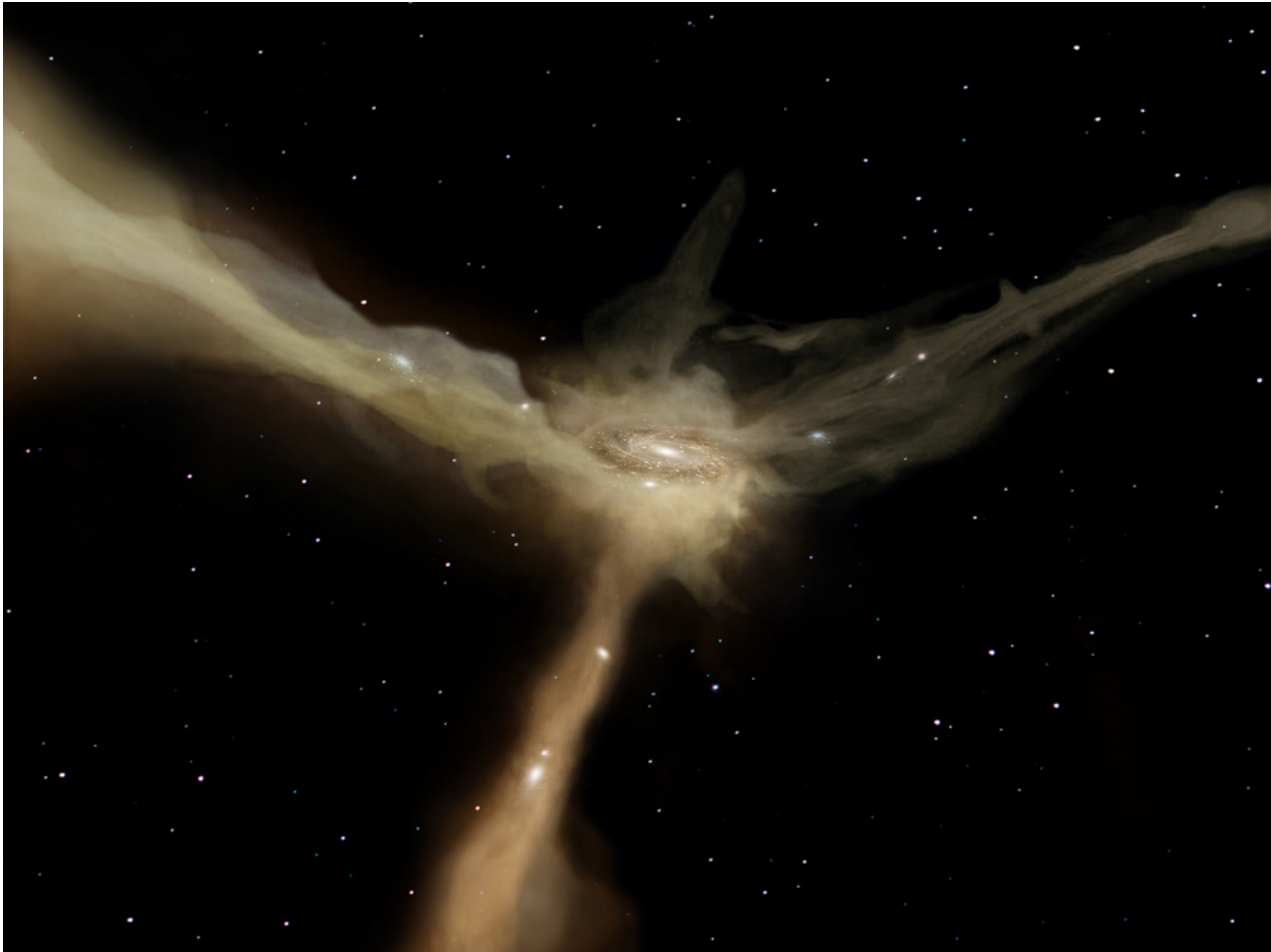








time=500



# Violent Disk Instabilities (VDI)

# Fast accretion rate and slow rates of star formation lead to violent disk instabilities (VDI)

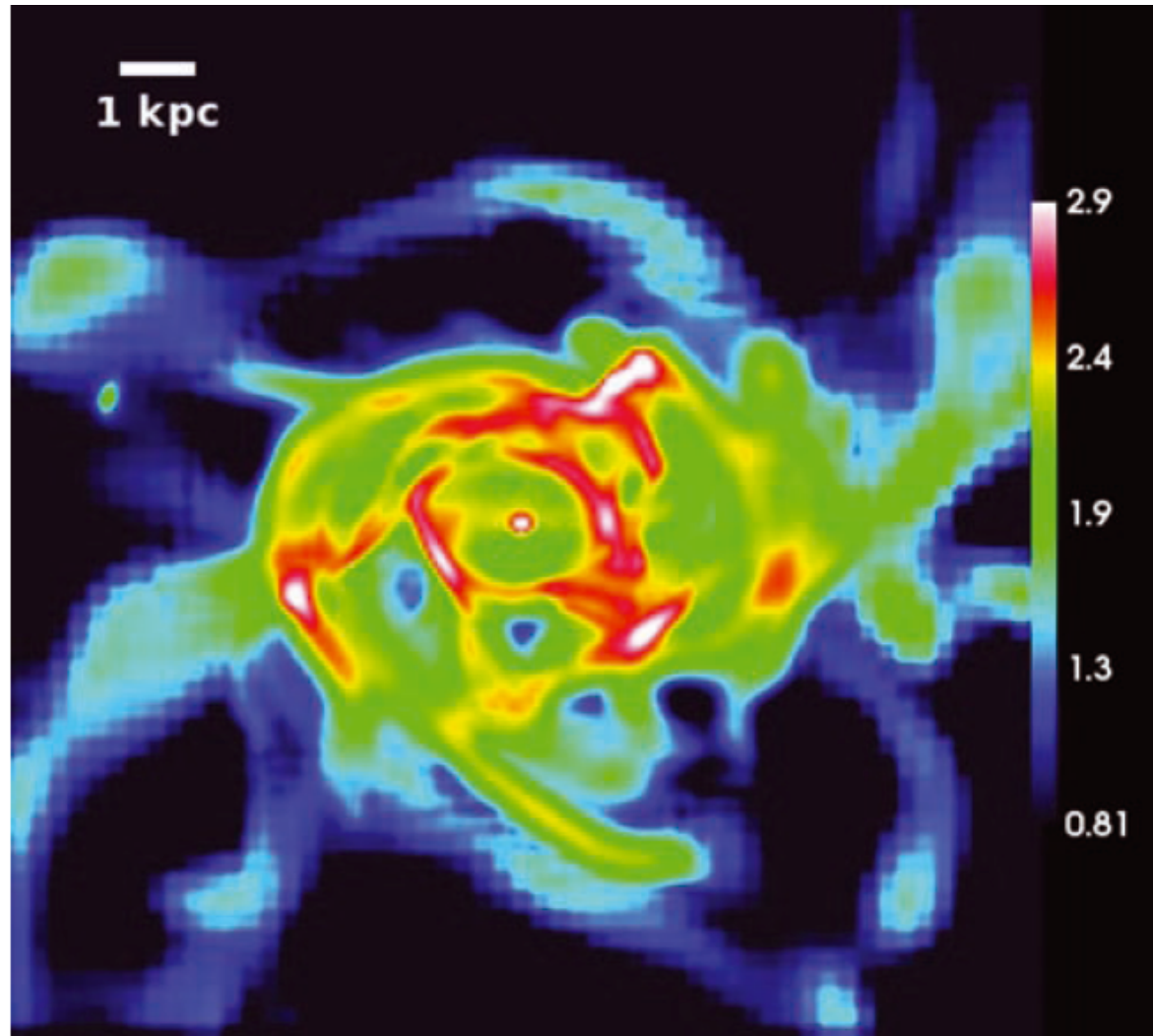
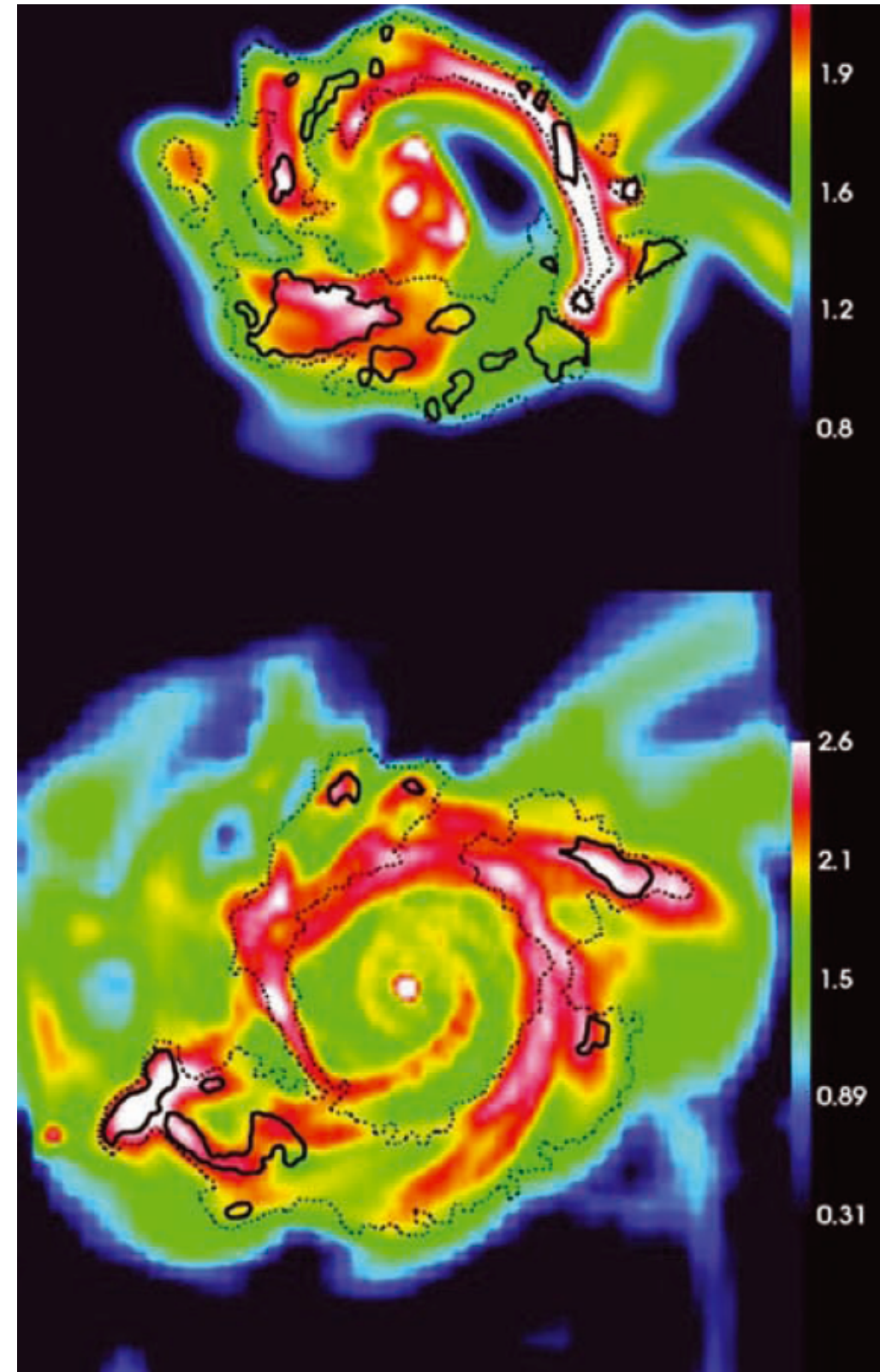
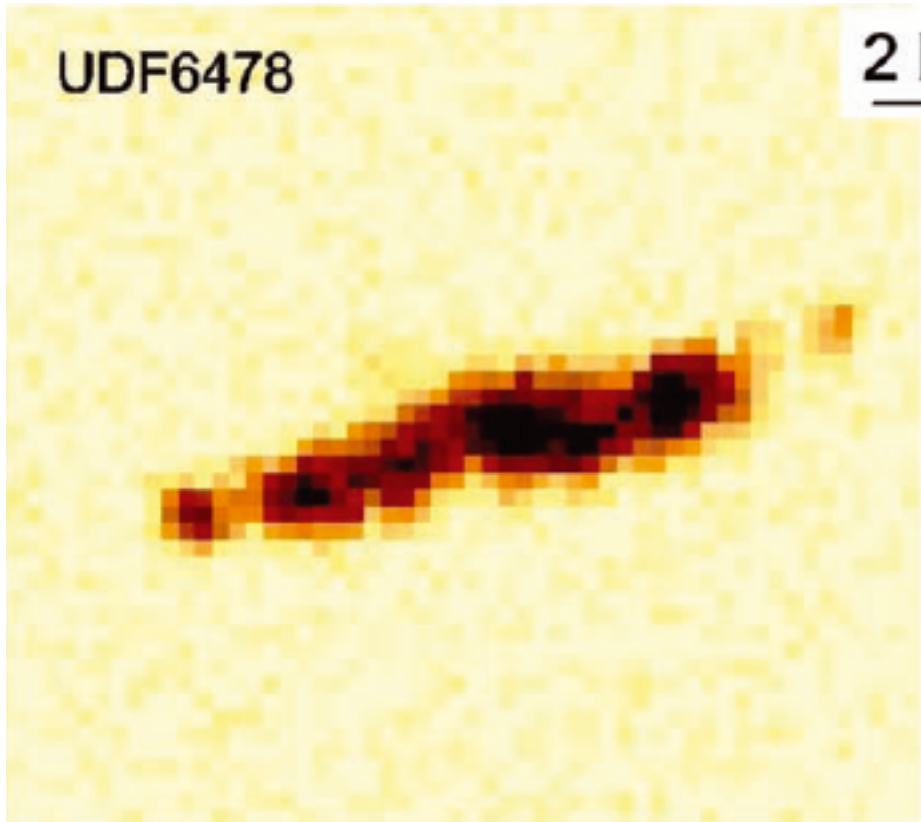


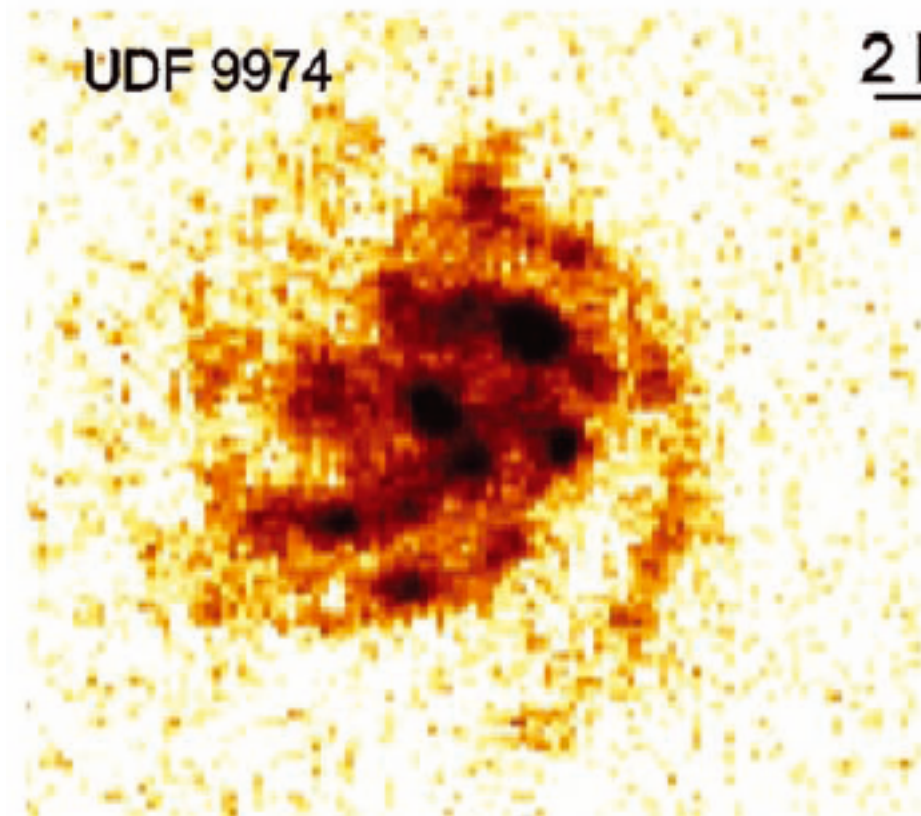
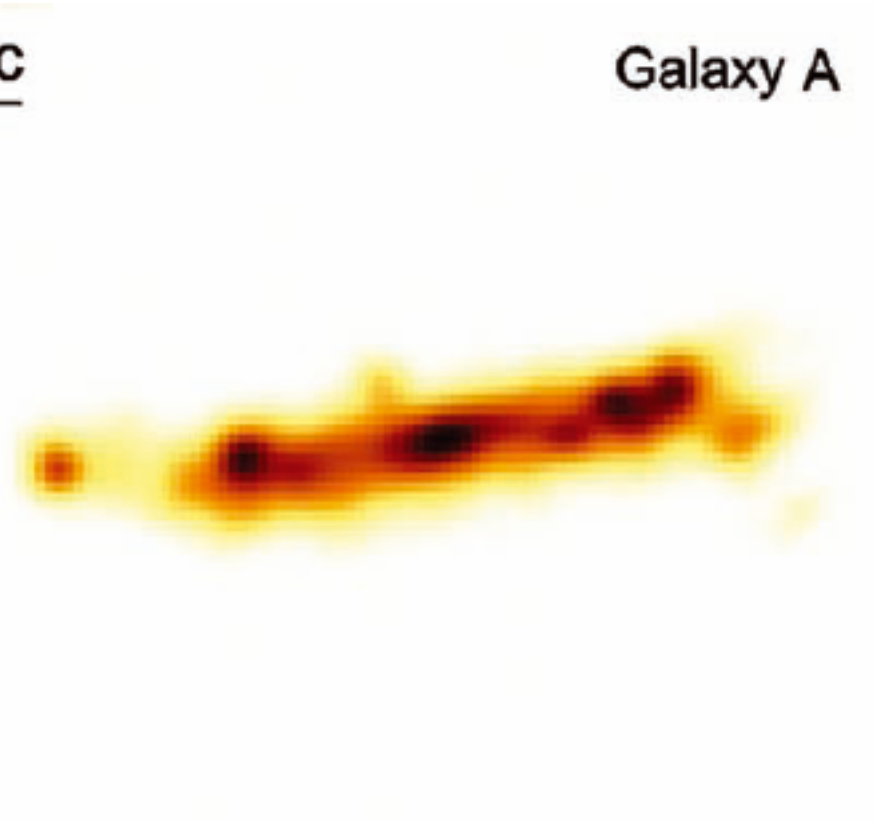
**Figure 1.** Face-on gas surface density in galaxy C at  $z = 2.1$ . The image demonstrates violent disc fragmentation into transient features and bound clumps, resembling observed SFGs and theoretical expectations. The size of the image is  $15 \times 15$  kpc. Surface density is in units of  $\log(M_{\odot} \text{pc}^{-2})$ . For comparison, the surface density of molecular clouds in low-redshift galaxies is  $\sim 100 M_{\odot} \text{pc}^{-2}$ .



Ceverino et al 2009



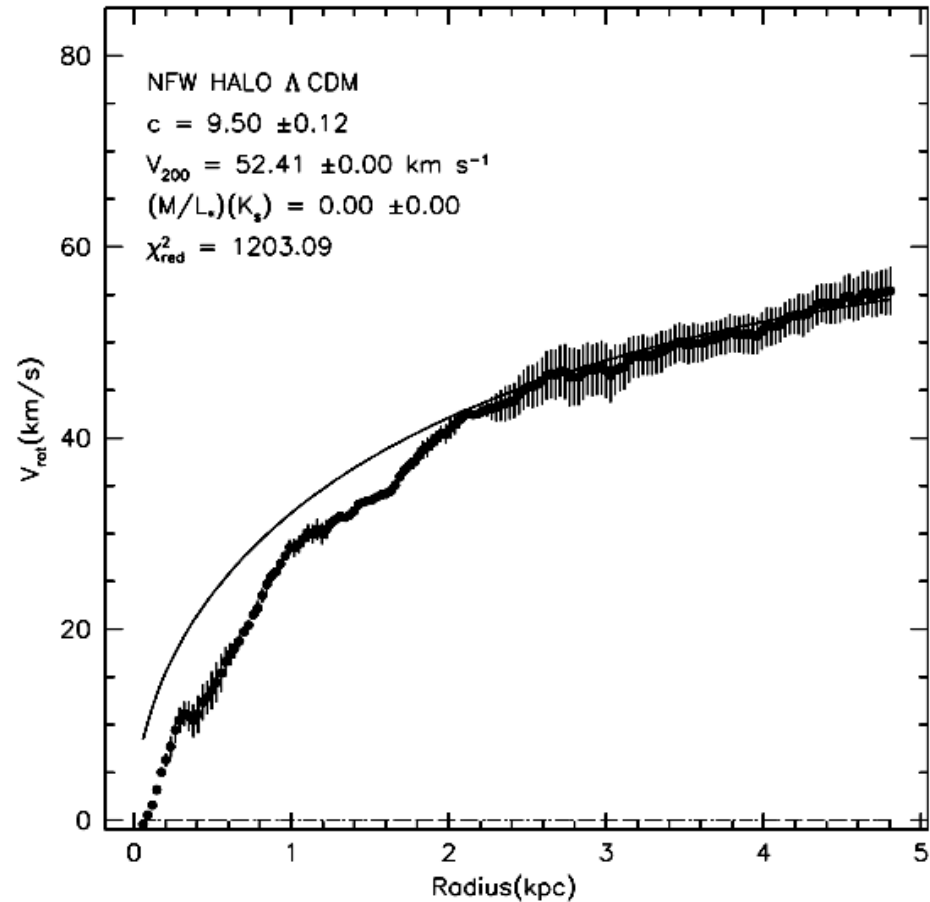
2 kpc



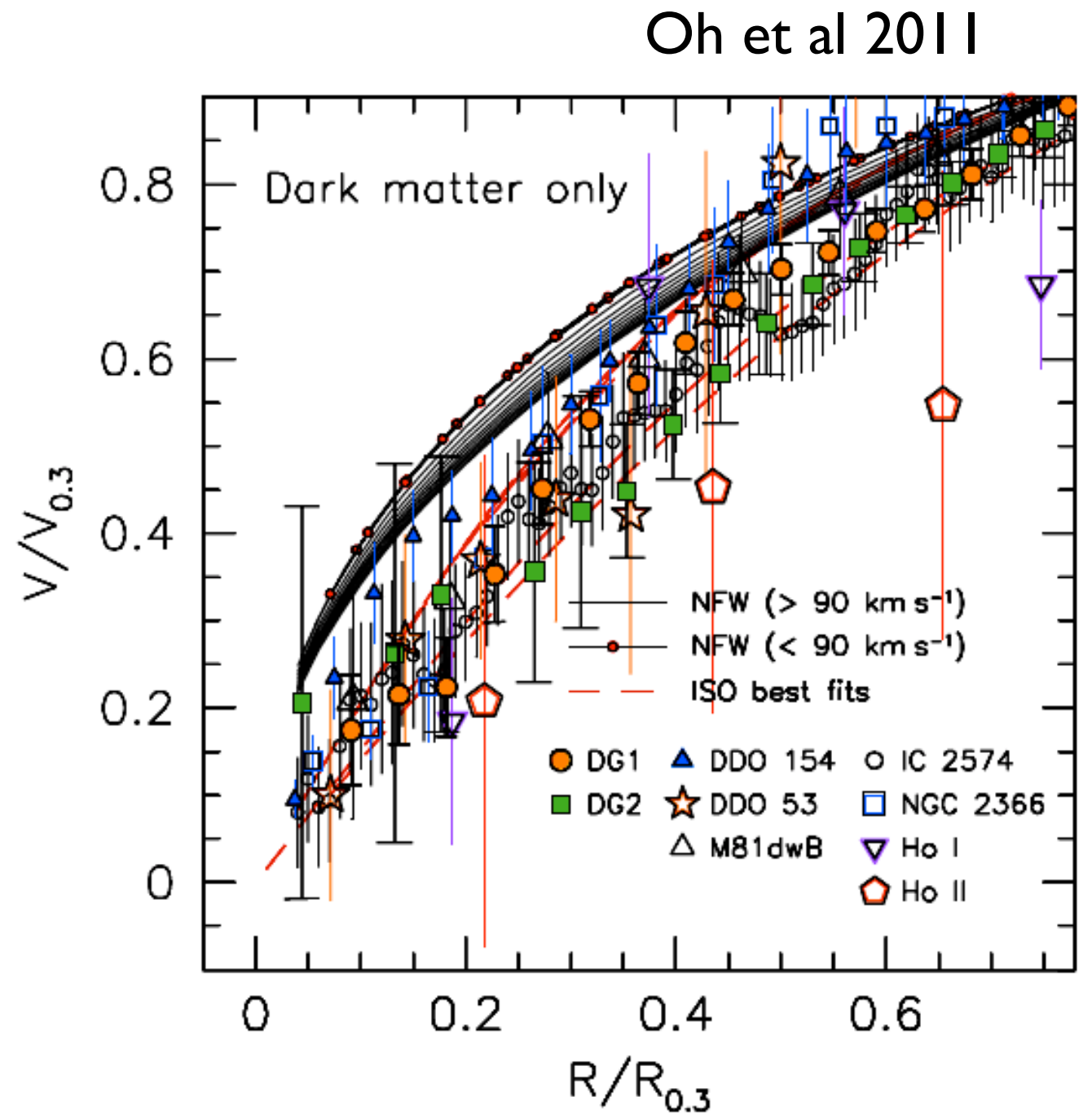
2 kpc



# Density Profiles: Mass at $\sim 1$ kpc radius. Core-cusp problem



NGC 6822, de Blok et al 2007



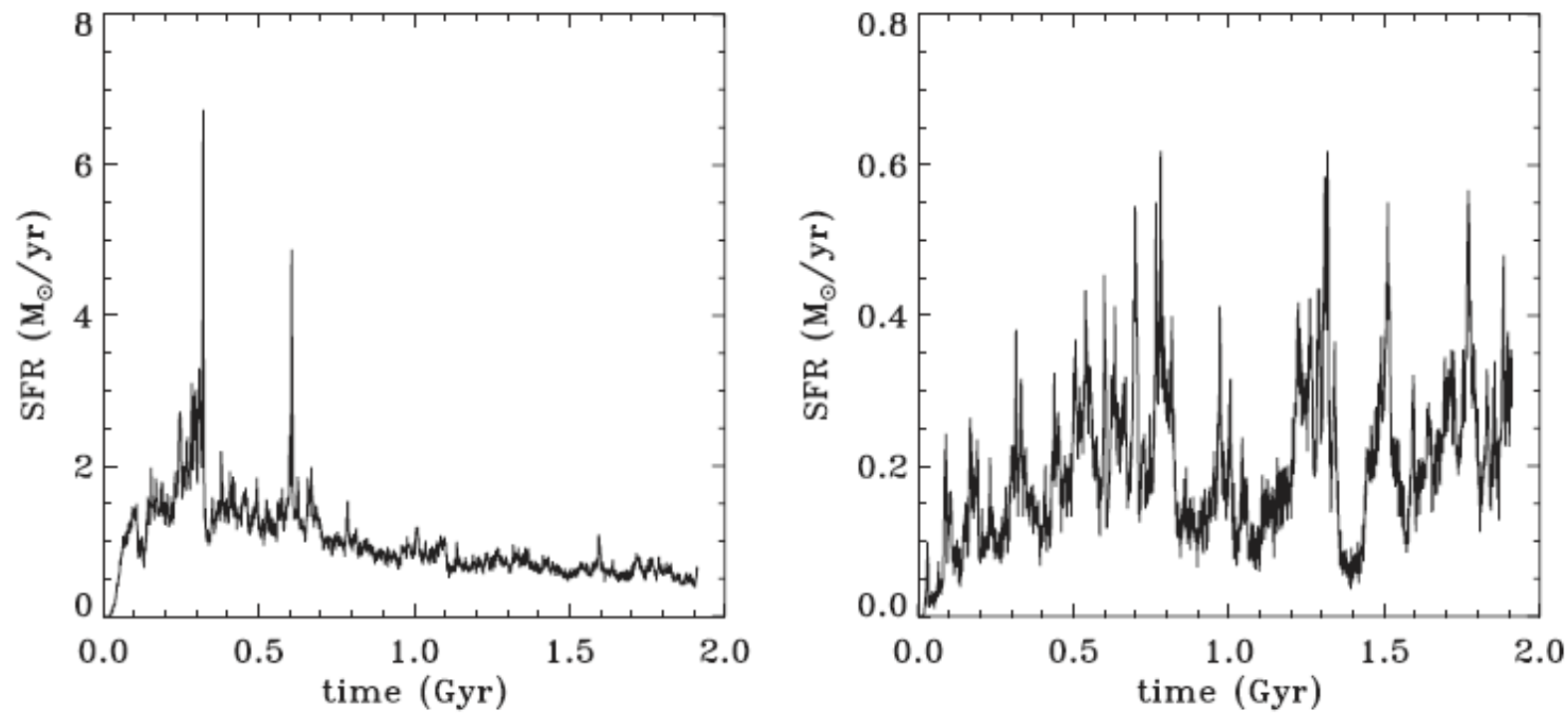


Figure 3. Star formation history in the runs without (left-hand plot) and with (right-hand plot) feedback.

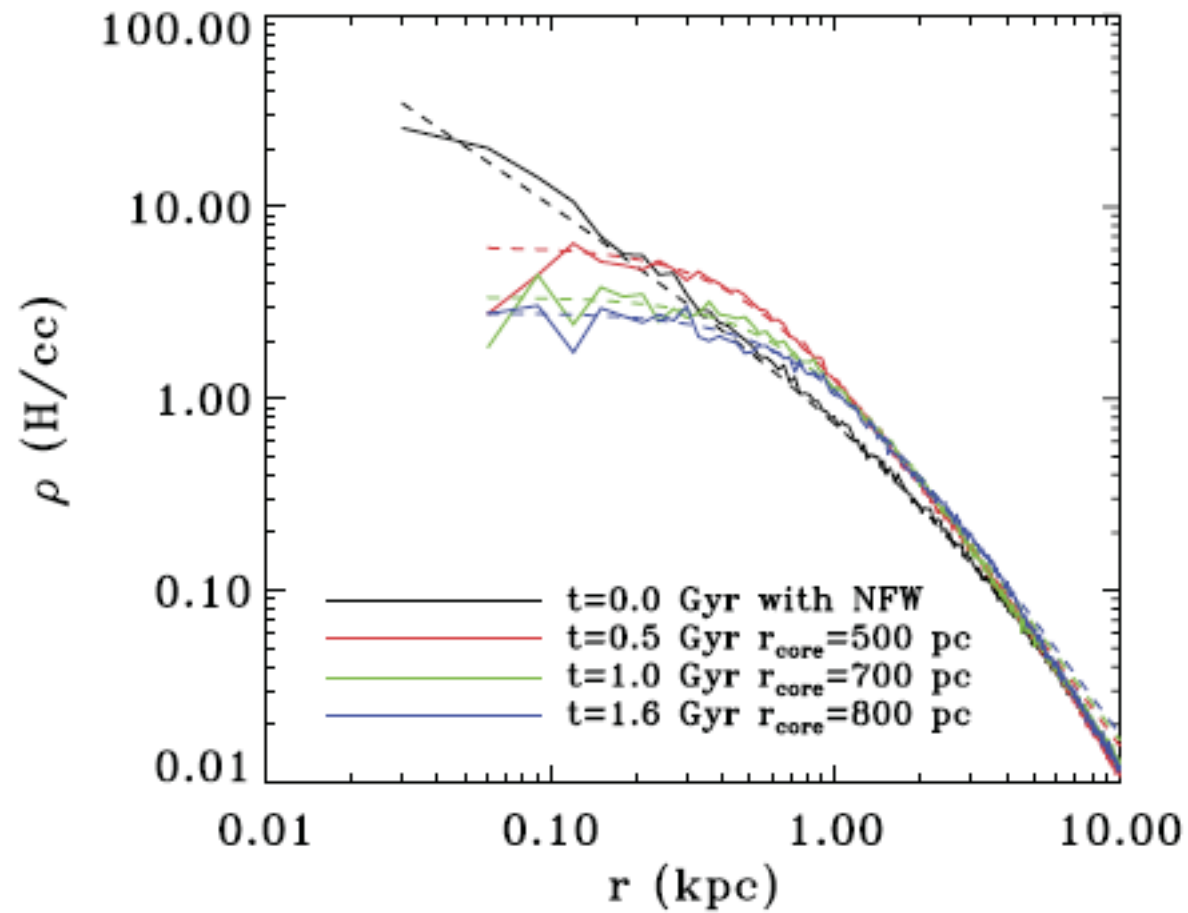
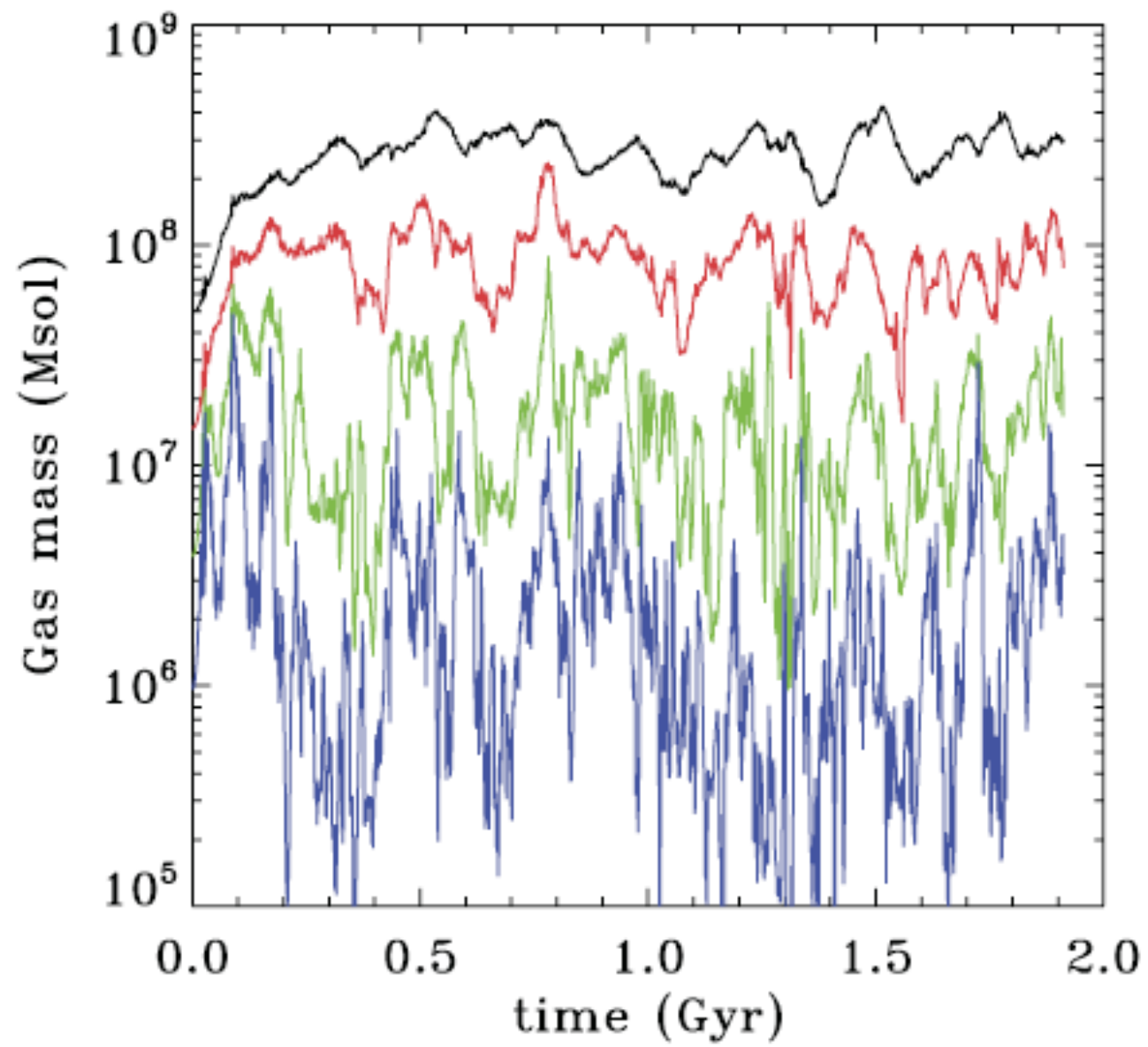


Figure 5. Evolution of the dark matter density profile over the 2Gyr of evolution for the control run with cooling, star formation and stellar feedback. We see the formation of a large core. We also show for comparison the analytical fit (dashed line) based on a pseudo-isothermal profile.



**Figure 7. Time evolution of the total enclosed gas mass within spheres of radii 200 (blue), 400 (green), 800 (red) and 1600 (black) pc for the simulation with feedback.**